GEO Newsletter

Group for Earth Observation

Group for Earth Observation **No 79 - September 2023**

This image, acquired by one of the Copernicus Sentinel-2 satellites at 9:00 UT on July 23, 2023, shows the extensive burn scar created by wildfires on the Greek island of Rhodes.

The massive wildfire devastated the holiday island, forcing the evacuation of some 19,000 people as the flames and smoke threatened homes and resorts.

GEO MANAGEMENT TEAM

General Information

John Tellick,

email: information@geo-web.org.uk

GEO Newsletter Editor

Les Hamilton,

email: geoeditor@geo-web.org.uk

Technical Consultant (Hardware)

David Simmons

email: tech@geo-web.org.uk

Webmaster and Website Matters

Vacancy

e-mail: webmaster@geo-web.org.uk

Management Team

David Anderson

Rob Denton

Nigel Evans: nigel.m0nde@gmail.com

Clive Finnis

Carol Finnis

Peter Green

David Simmons

David Taylor

Useful User Groups

Weather Satellite Reports

This group provided weekly reports, updates and news on the operational aspects of weather satellites.

https://groups.io/g/weather-satellite-reports

SatSignal

This end-user self help group is for users of David Taylor's Satellite Software Tools, including the orbit predictor WXtrack, the file decoders GeoSatSignal and SatSignal, the HRPT Reader program, the remapper GroundMap, and the manager programs - MSG Data Manager, GOES-ABI Manager, AVHRR Manager etc.

https://groups.io/g/SatSignal

MSG-1

This forum provides a dedicated area for sharing information about hardware and software for receiving and processing EUMETCast data.

https://groups.io/g/MSG-1

GEO-Subscribers

This is the official group is for subscribers of the Group for Earth Observation (GEO), aimed at enthusiasts wishing to exchange information relating to either GEO or Earth Observation satellites.

https://groups.io/g/GEO-Subscribers/

Follow GEO on Twitter and Facebook

Group for Earth Observation

Receive the latest news from EUMETSAT, ESA, NOAA, NASA, and the Met Office etc. through their Twitter feeds ...

https://twitter.com/geo_earth_obs

Visit GEO on facebook and link to dozens of news items from NOAA, NASA, ESA, EUMETSAT and much more ...

http://www.facebook.com/groupforearthobservation

From the Editor

Les Hamilton

After the Earth experienced the hottest month of July ever recorded, and wildfires of hitherto unrecorded magnitude were springing up throughout Europe and The Americas, probably exacerbated by the start of a new El Niño cycle, it will come as little surprise that many of this quarter's articles reflect this.

As was hinted in the previous Newsletter, Meteor M No 2-3 was launched in late July and, unusually, started transmitting visible imagery the day after gaining orbit. But as the article on page 4 explains not everything has gone to plan. Admittedly the craft is still in commissioning mode, and hopefully its teething troubles will soon be a thing of the past.

For enthusiasts making use of BUFR data from EUMETcast, Richard Osborne builds on his previous articles to describe his experiments to determine the best way to visualise their data.

Contents

Russia's Meteor M No 2-3 takes to the Skies

Les Hamilton

June 27, 2023 was the day that weather satellite enthusiasts around the world had been anticipating for years, when Russia's **Meteor M 2-3 satellite** finally launched successfully. Built in 2016, the satellite was originally slated for a late 2020 launch, but the date continually lapsed through lack of finance until activity at the Vostochny Cosmodrone early this year indicated that its launch might be imminent. As with earlier satellites in the series, this three tonne craft was designed to observe global weather, the ozone layer and ocean surface temperatures, as well as ice conditions in order to facilitate shipping in the Arctic Ocean. Meteor M 2-3 differs from its predecessors by the addition of a deployable phased-array radar antenna for all-weather scanning of the Earth.

Unlike previous satellites in this series, which did not transmit imagery for several weeks following launch, Meteor M 2-3 was disseminating RGB123 images on both LRPT and HRPT frequencies within 24 hours of attaining orbit. And as a two-day conflict with NOAA 19 was looming, the transmission frequency was initially 137.90 MHz which avoided conflict. As is normal with a new launch, there were no transmissions on the infrared channels at this time as it takes several weeks before the radiometers cool down sufficiently to operate effectively.

Commissioning Phase

Because there is an initial commissioning phase, possibly lasting up to six months, the transmission parameters of Meteor M 2-3 have been in a continued state of flux: frequency has swapped between 137.10 MHz and 137.90 MHz numerous times and the Symbol Rate has done likewise, oscillating periodically between 72 000 and 80 000 symbols per second (i.e. baud rate).

Following launch, initial images were encouraging and figure 6 on the following page shows one of the earliest images I acquired, on July 1, and is essentially flawless.

But it soon became apparent that all was not well as reports from around the globe indicated that the satellite's LRPT signal strength was unexpectedly low, only about half that anticipated. Additionally, the images were frequently ruined by the presence of randomly distributed horizontal black bands, often considerably wider than the intrusive black bands so characteristic of the now defunct Meteor 2M satellite, as illustrated the LRPT Decoder window screenshot shown in figure 4. Frustratingly, this image dropout was not accompanied by signal loss as the acquisitions in SDRSharp maintained lock throughout the passes (figure 5).

My station is located in Aberdeen, Northeast Scotland, and while I obtained good coverage from at least as far north as Tromsø in Norway, it was clear that the signal from Meteor dropped off rapidly after the satellite passed zenith on its southward track, and imaging rarely extended

Figure 1
The payload section with the Fregat space tug, Meteor-M2-3 satellite and secondary payload being prepared for encapsulation under its payload fairing.
Image: Roscosmos

Figure 2
The Soyuz-2-1b launch vehicle on the launch pad, prior to take-off on the morning of June 24, 2023.
Image: Aerospace Capital

Figure 3
The Soyuz-2-1b launch vehicle taking off from Vostochny Cosmodrone at 14:34:49 Moscow Time on the morning of June 24, 2023.
Image: Aerospace Capital

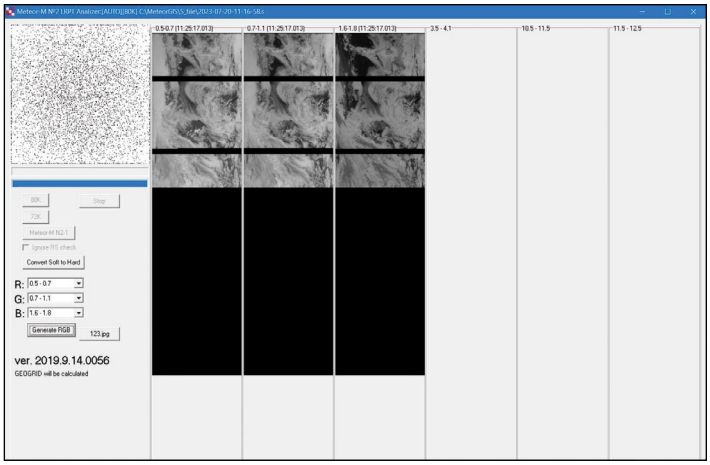

Figure 4 - Problem bands during image acquisition

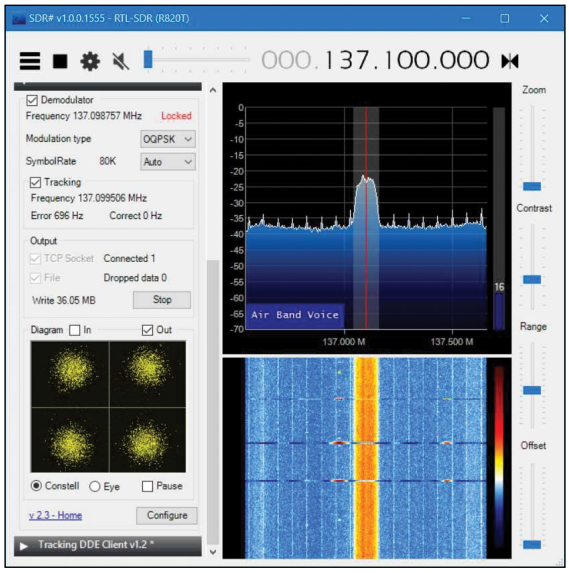

Figure 5 - Signal lock maintained despite image dropout

farther south than the English Channel. This was a pattern reported by observers from around the globe and the consensus seemed to be that, in all probability, the QFH transmission antenna aboard Meteor M 2-3 had failed to deploy fully. My best images always come from passes where Meteor is west of the observing station,

Readers with long memories may recall a similar situation when NOAA 15 was launched in May 1998: for the first month or so, imagery was restricted, also attributed to incomplete deployment of the APT antenna. Then suddenly, several weeks later, the problem suddenly resolved itself. It was posited that the repeat expansion and contraction resulting from the heating/cooling cycle as NOAA 15 orbited Earth between sunshine to darkness had triggered the antenna's full deployment.

On July 25, 2023, the testing of Meteor M 2-3's MSU-MR (VIS/IR Imaging Radiometer) infrared sensors commenced. Early images were confusing and showed almost no deliniation between land and cloud. Not only did the 'black band problem' seem to become worse by the day, there were now frequent unheralded switches of the Frequency and Symbol Rate, resulting in many passes being missed altogether.

In theory, frequency switching between 137.10 MHz and 137.90 MHz could be utilised to great effect if it were

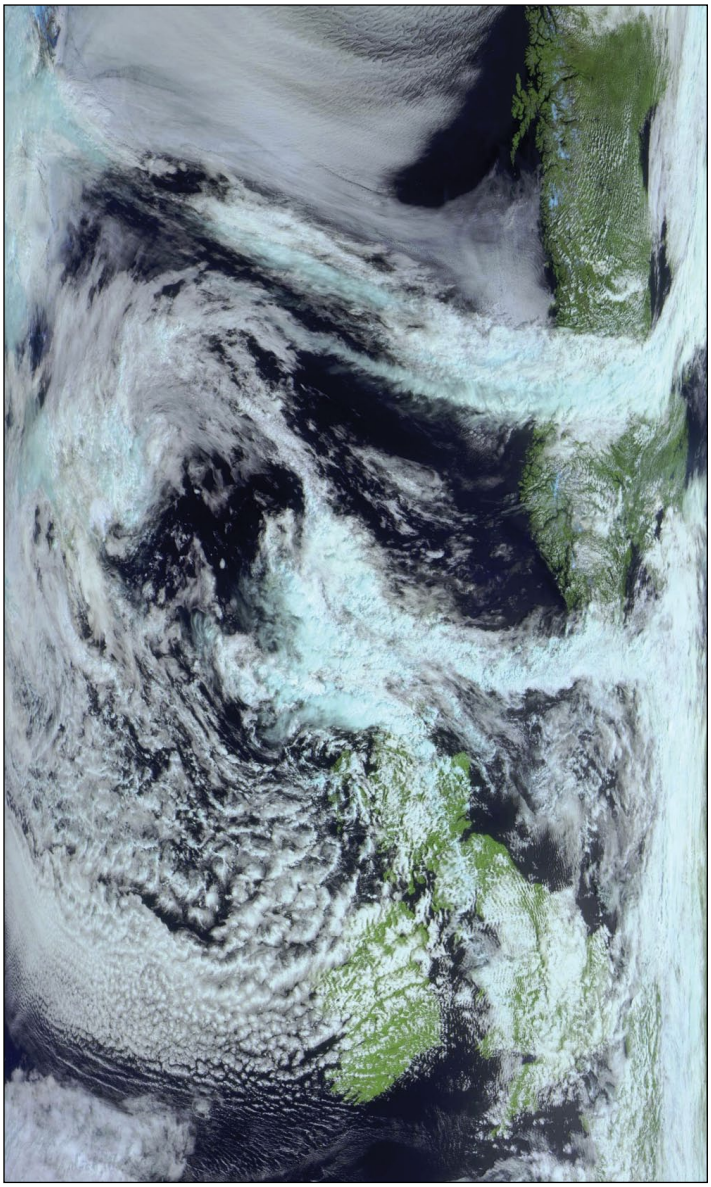

Figure 6
This southbound Meteor M2-3 RGB123 image acquired on July 1, 2023 shows excellent coverage to the north but is seriously curtailed at the English Channel to the south.

done to avoid the periods of conflict when the footprint of Meteor 2-3 overlaps with those of the NOAA 18 and NOAA 19 satellites. But in practice, the very reverse seems to be the case as a frequency change that could have avoided such a conflict is often actioned a day or two after said overlap has ended.

But of course, we must recognise that Meteor M2-3 is still not fully commissioned and is still a work in progress. Hopefully, better times may still lie ahead.

On a happier note, the operators restored the three visible channels on August 12 to provide users with colour composite imagery once more. And although the 'black band problem' has not been totally resolved, there do seem to be more clean passes than hitherto (see the Meteor M2-3 image on page 40).

And now some good news. It has been reported that a sister craft, Meteor M No 2-4, could well be orbited in December this year.

The altered life of GOES-3

GOES-3: The Weather Satellite that Refused to Retire

Carl Reinemann - https://usradioguy.com/

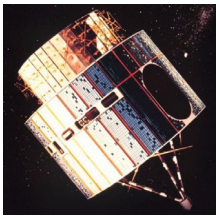

GOES-3, which became NOAA's third Geostationary Operational Environmental Satellite (GOES) after it was placed into orbit on June 16, 1978, made history when it reached the end of its life and was decommissioned on June 29, 2016. After 38 years, and a second life as a communications satellite, GOES-3 became one of the oldest continuously operating satellites ever.

GOES-3 was launched aboard a Delta 2914 carrier rocket, and used a Visible/Infrared Spin Scan Radiometer (VISSR) to provide day and night observations of cloud and surface temperatures, cloud heights, and wind fields. Although the craft was spin-stabilized, and consequently only actually viewing Earth less than 10% of the time, and providing data in only two dimensions, GOES-3 provided forecasters with some of their first near real-time looks at atmospheric conditions from a fixed location.

Serving from the 'GOES-West' position until the late 1980s, GOES-3 monitored and measured Earth's weather systems for a decade. The satellite's most famous imagery was captured on May 18, 1980, when the Mount St Helens volcano erupted, spewing ash over Washington State. NOAA relied on data and imagery from GOES-3 to track the dispersal of ash clouds from the eruption in order to warn airline pilots flying in the area of the potentially deadly hazard.

This NOAA GOES-3 Visible (0.65 µm) image shows the volcanic cloud shortly after the explosive eruption of Mount St Helens on May 18, 1980
CREDIT: https://cimss.ssec.wisc.edu/satellite-blog/archives/

Once GOES-3 had outlived its useful life as a prime weather satellite, the craft was used as a backup for other operational weather satellites in the GOES series, specifically as a backup for GOES-4 at a time when it experienced problems with its imager and was unable to provide weather data. Eventually, in 1989, the weather-observation instruments aboard GOES-3 failed completely, but that was by no means the end of this satellite's story.

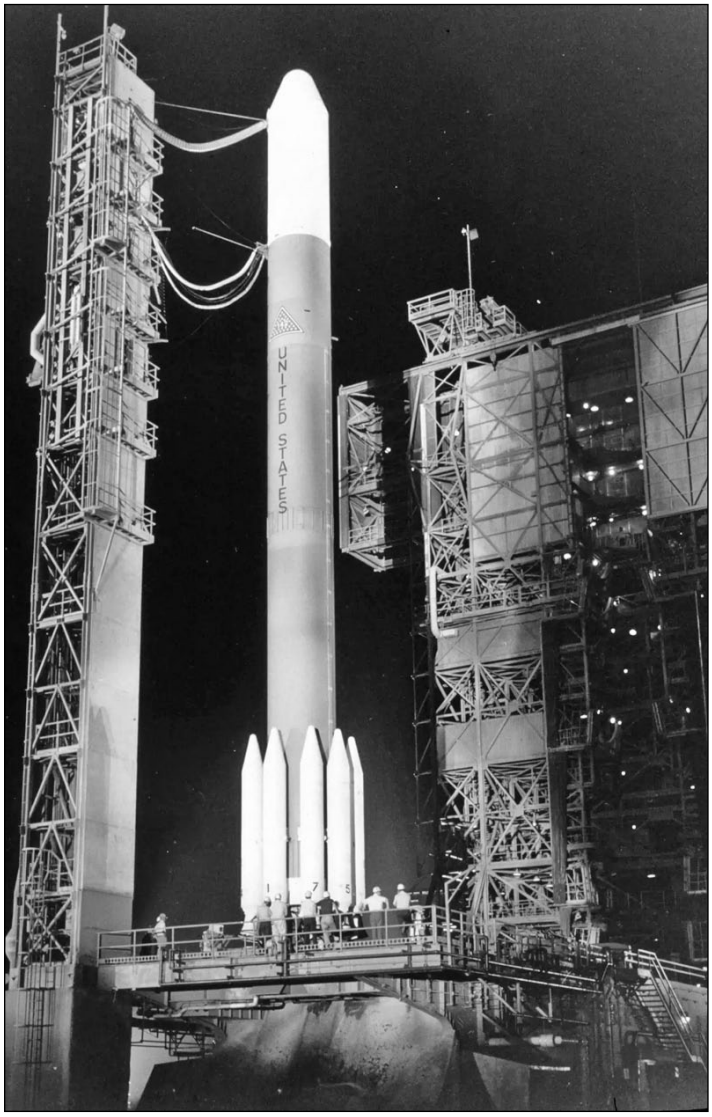

GOES-C (GOES-3 once operational) awaiting launch
Credit: NASA

Although its imager could no longer capture weather imagery, GOES-3 still had the ability to send and receive data from geostationary orbit. This realisation caught the attention of PEACESAT [1] (the Pan-Pacific Education and Communications Experiments by Satellite Program), who hatched a plan to repurpose GOES-3 as a communications satellite.

From 1988 right until the early 1990s, GOES-3 served as a communication lifeline to islands in the Pacific Ocean region, utilising the S-Band to L-Band translator aboard the satellite (originally used for the rebroadcasting of ground-processed GOES-3 image products to end users). This service established reliable internet and telecommunications access to the Pacific Islands and provided healthcare services, educational programs,

disaster management, response aid and many other public services.

By 1995, with the depletion of GOES-3's station-keeping fuel, the satellite started straying from its original equatorial location. As the inclination of GOES-3's orbital plane with respect to Earth's equator drifted higher and higher, this unique, high-inclination orbit allowed GOES-3 to make direct radio connection between Earth's polar regions and the United States for up to 6.5 hours a day. This rare capability caught the eye of the National Science Foundation (NSF).

As a result, GOES-3 changed hands to provide a new critical communications link—this time, for the South Pole. Through a series of agreements, NOAA permanently transferred the satellite from PEACESAT to the NSF in order that it be used for direct digital communications between the continental USA and the Amundsen-Scott South Pole Station.

Since 1995, GOES-3 has been one of the main satellites used to communicate with, and provide internet service to, the Amundsen-Scott South Pole Station and a variety of deep-field science locations in the Antarctic. So Facebook posts, Tweets, emails and so on received in the USA from the south pole were achieved using an item of hardware that's over 30 years old.

Amundsen-Scott's extreme latitude—90° degrees south, directly over the pole—places it outwith the range of equatorial geostationary communications satellites. But GOES-3's oscillating orbit periodically shifted it far enough south to communicate with the southernmost point of the planet for around 6½ hours per day. The South Pole Station relies on satellite links for communication with the rest of the world and GOES-3, which could provide approximately 1.5 MB/s, was sufficient for the station's needs at that time. The South Pole Station communicated with GOES-3 using the 9-metre South Pole Marisat-GOES Terminal.

Over the years, the South Pole has relied on a number of different satellites for communication links. However, GOES-3 remained a key part of the station's infrastructure for more than two decades, providing a reliable and consistent connection to the outside world, even in the harshest of conditions.

One researcher explained that, with only 1.5 megabits of data link shared throughout the entire station—for voice as well as data—traffic had to be prioritised: voice communications first, then higher priority data such as scientific payloads, and finally normal web surfing. The experience was definitely a bit frustrating to use, but considering their spot down at the South Pole, it's incredible that they were able to get anything at all. In one case, downloading a PDF document for an arctic tractor repair manual, took two days because of the low bandwidth and limit of 6½ hours daily coverage. In satellite reception terms, that's like receiving data when pointing the dish at about 1° to 3° in elevation!

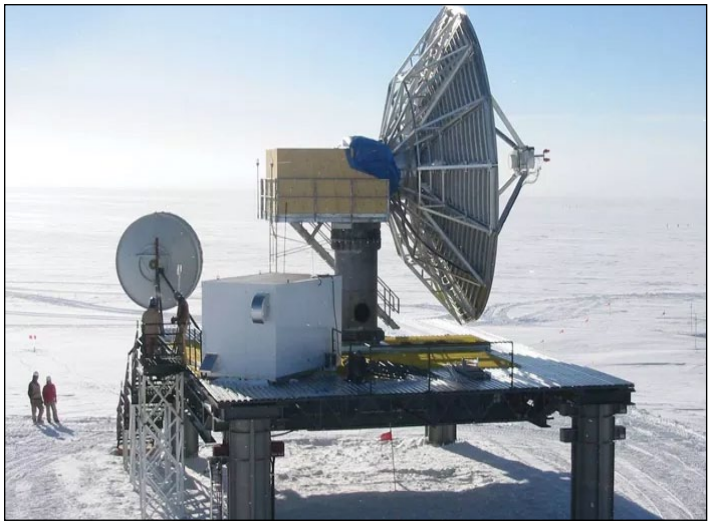

The platform bearing the 9-metre South Pole Marisat-GOES Terminal, photographed prior to its enclosure under a radome in 2002, along with the smaller GOES-3 backup antenna.
Photo: National Science Foundation

For over 20 years, the South Pole relied on the GOES-3 weather satellite for communication links with the outside world, but in 2016, GOES-3 was finally decommissioned after 38 years in operation. While the satellite had served its purpose admirably, it was no longer capable of meeting the demands of modern communication needs. It was replaced by a newer satellite, which provided higher bandwidth and more advanced capabilities.

Decommissioning took 20 orbital manoeuvres over 14 days during which the satellite was carefully nudged into a 'graveyard' orbit, some 250 kilometres above current operational geostationary satellites. Once there, and ensuring that all fuel on-board had been depleted, all the satellite's systems were shut down.

The decommissioning phase ended on June 29, 2016, placing GOES-3 in the history books as the 'One of the Oldest Continuously Operating Spacecraft in History' after a service life of 38 years and 13 days.

Reference

1 PEACESAT (http://peacesat.hawaii.edu/)

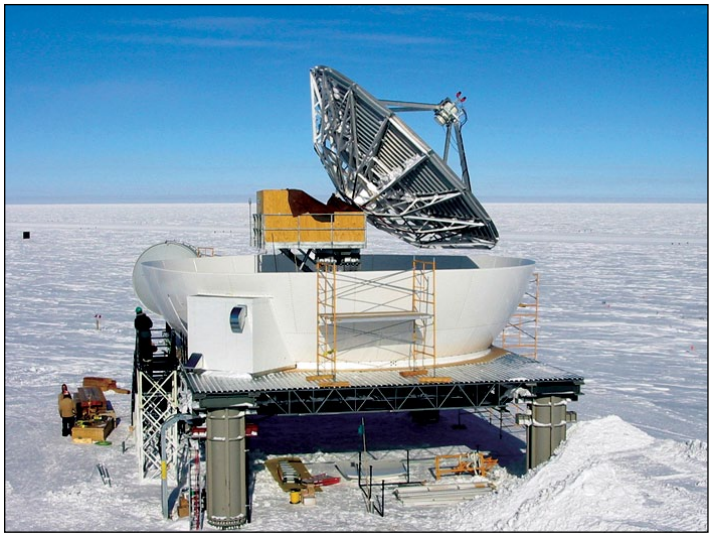

The antenna was enclosed under a protective radome, circa 2002
Photo: National Science Foundation

Storm Poly Ravages the Netherlands

Copernicus Image of the Day

https://www.copernicus.eu/en/media/image-day

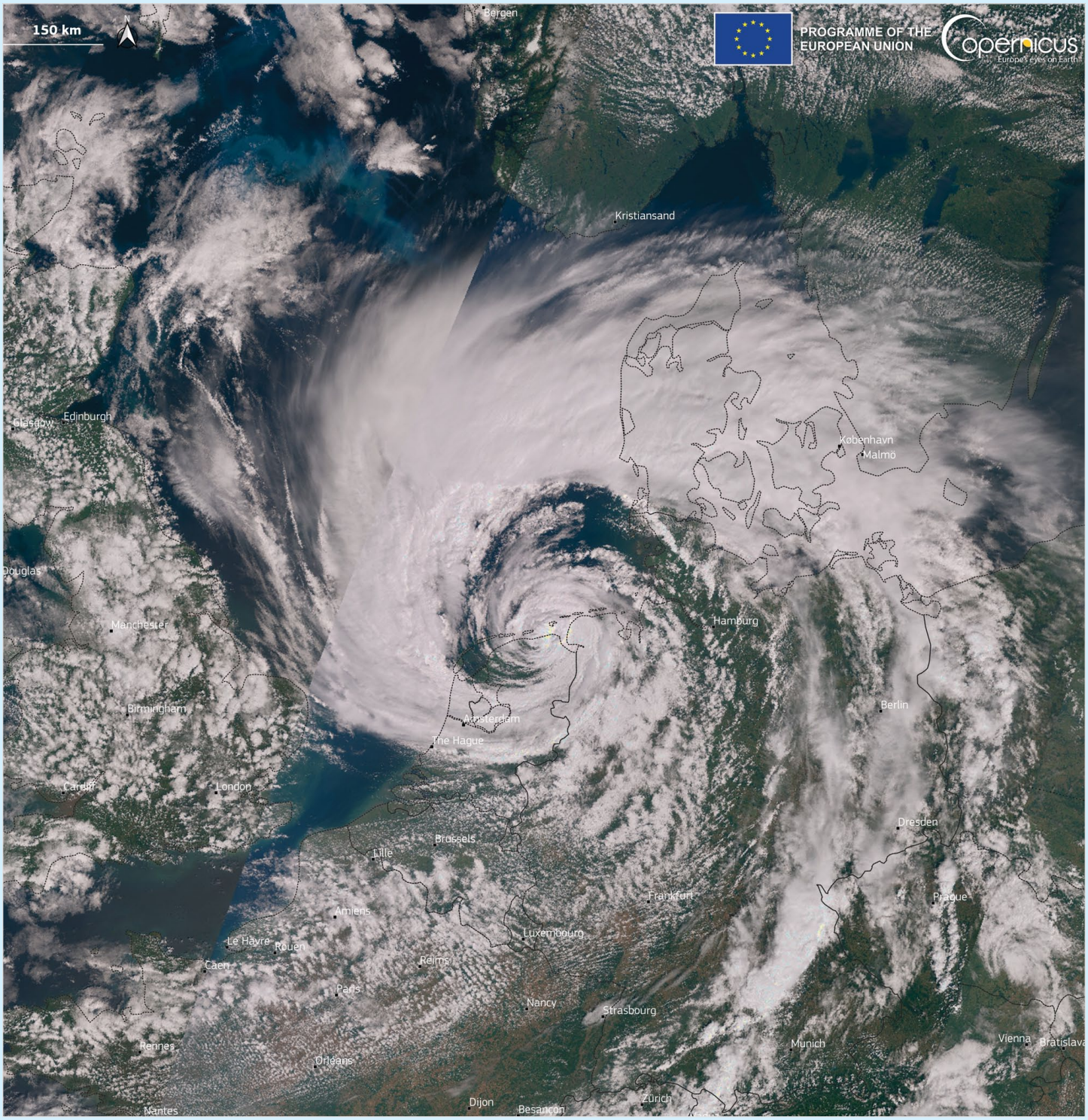

Credit: European Union, Copernicus Sentinel-3 imagery

Acquired on 5 July 2023, this Copernicus Sentinel-3 image reveals a wide view of Storm Poly raging across the Netherlands. With wind gusts of 146 km/h, it was the strongest summer storm on record for the country.

It caused widespread tree damage, prompting Dutch authorities to issue warnings advising people to remain indoors. Air and train transportation were significantly disrupted, with more than 300 flights being cancelled at Amsterdam Schiphol airport.

The Copernicus satellites provide a vast amount of data that enable the monitoring of extreme weather events such as hurricanes, cyclones, and storms, as well as their consequences.

California Reservoir Rebound

NASA Earth Observatory

Story by Lindsey Doermann

Shasta Lake, California's largest reservoir, filled to nearly 100% capacity in May 2023, reaching levels not seen for four years. Since 2019, a prolonged period of extreme drought had resulted in dwindling reservoir levels. In the early months of 2023, heavy rains and meltwater from an above-average mountain snowpack caused a notable turnaround.

The rising water level is apparent in the image pair opposite, which shows Shasta Lake on November 18, 2022 and May 29, 2023. On November 18, the lake stood at 31% capacity, according to the *California Department of Water Resources* (DWR). By May 29, it was 98% full, and the tan fringe, or 'bathtub ring', around its perimeter had vanished. The images were acquired by the Operational Land Imager (OLI) on the Landsat 8 (figure 1) and the OLI-2 on Landsat 9 (figure 2).

The series of images in figure 3 (overleaf) shows the progression of the lake's rebound. A thin bathtub ring was still visible on January 29, 2023, when the OLI-2 acquired the centre image. On that day, the lake stood at 56% of capacity, or about 87% of the historical average for that time of year.

The colour of the water in the centre image probably appears greener because of suspended sediment. In the right-hand image, some portions of the lake surface appear lighter due to an optical phenomenon known as sunglint, and suspended sediment may also be present.

Lake Oroville, the state's second-largest reservoir, was also near capacity on May 29, at 97% full. Both Lake Oroville and Shasta Lake are critical, not only for water storage, but also for flood control, recreation, irrigating cropland in the Central Valley, and preventing saltwater intrusion into the Sacramento-San Joaquin Delta.

Figure 1 - Shasta Lake imaged on November 18, 2022
NASA Earth Observatory image by Lauren Dauphin, using Landsat data from the U.S. Geological Survey.

Figure 2 - Shasta Lake imaged on May 29, 2-23
NASA Earth Observatory image by Lauren Dauphin, using Landsat data from the U.S. Geological Survey.

Full reservoirs do not ensure plentiful water for years into the future. The past four years have been a testament as to how drastically reservoirs can change over the course of one or two years. In addition to the many demands for water, lake levels need to be drawn down to create capacity for flood control in wetter seasons. The California DWR is collaborating with other agencies to incorporate better forecasting and observation technologies in order to optimise water releases.

Plentiful surface water does not necessarily equate to replenished groundwater stores. In California's Central Valley, groundwater may account for two-thirds of agricultural water use during drought years. A recent study using data from NASA's Gravity Recovery and Climate Experiment (GRACE) and GRACE Follow-On satellite missions found that groundwater depletion in the Central Valley has been accelerating since 2003.

Officials in California are working to leverage the recent influx of water. While some groundwater recharge happens naturally, resource managers can employ other strategies to send water underground, such as diverting it into canals or ponds and injecting it into the subsurface through wells.

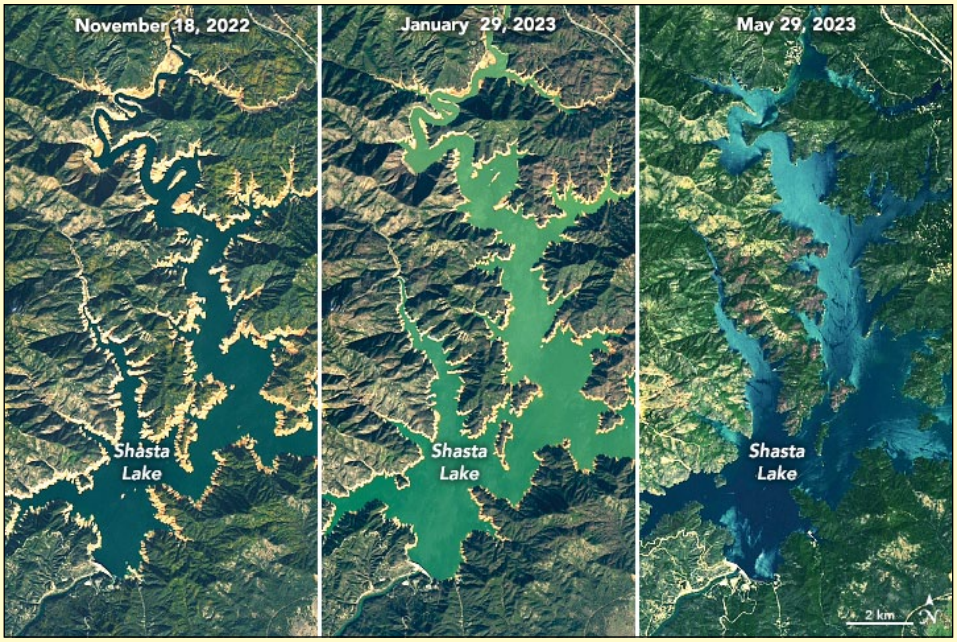

Figure 3 - The filling progression of Shasta Lake
NASA Earth Observatory image by Lauren Dauphin, using Landsat data from the U.S. Geological Survey.

EU's Third Largest Suspension Bridge Inaugurated in Romania

Copernicus Image of the Day

This image, acquired by one of the Copernicus Sentinel-2 satellites on 8 July 2023, shows the newly commissioned Braila Bridge in Romania. At nearly 2 kilometres in length, it is the third longest suspension bridge in Europe. It will reduce travel times, vehicle operating costs, exposure of residents to air and noise pollutants, and improve the quality of life along the access routes to Danube crossing points in Braila and Galati. The construction of this bridge was funded by the EU with €363 million from Cohesion Policy funds. The bridge was opened on 6 July 2023.

Credit: European Union, Copernicus Sentinel-2 imagery

El Niño Returns

NASA Earth Observatory

Story by Kathryn Hansen

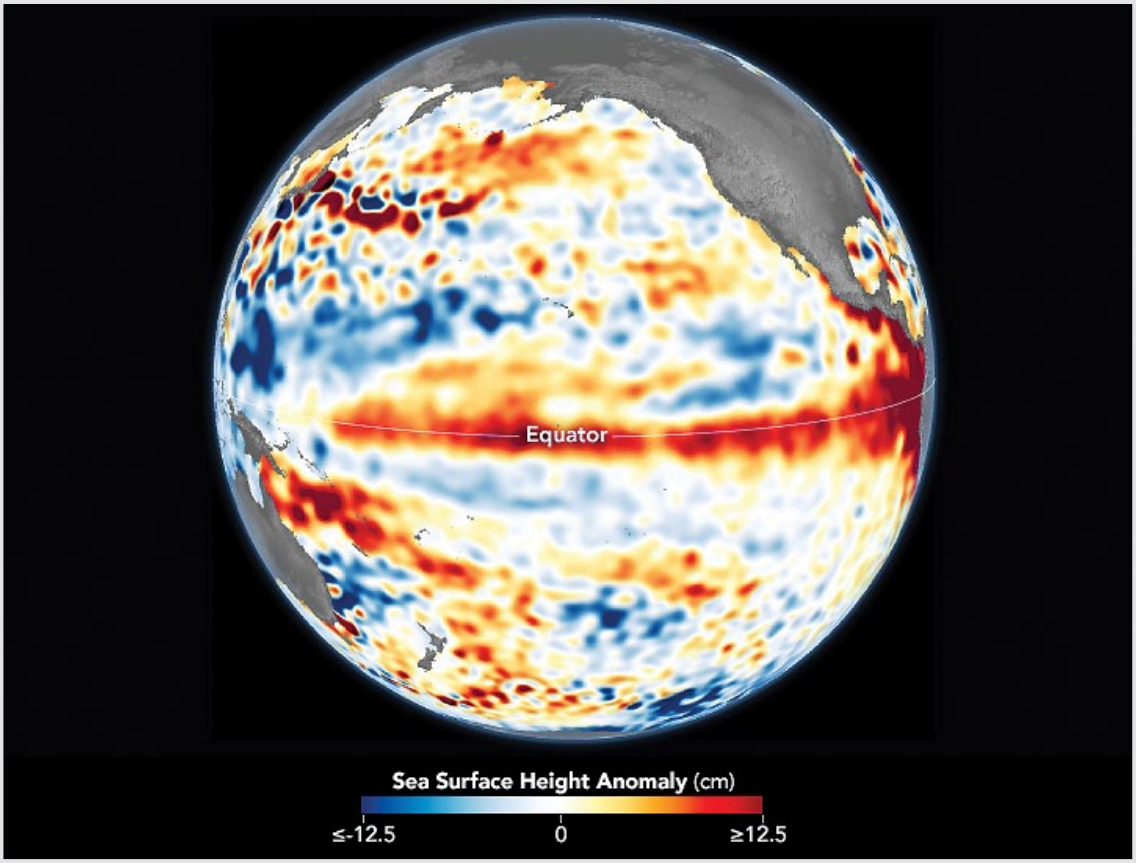

NASA Earth Observatory image by Lauren Dauphin, using modified Copernicus Sentinel data (2023) processed by the European Space Agency and further processed by Josh Willis, Severin Fournier, and Kevin Marlis/NASA/JPL-Caltech.

After three consecutive years of La Niña, spring 2023 saw the return of El Niño—a natural climate phenomenon characterized by the presence of warmer than normal sea surface temperatures (and higher sea levels) in the central and eastern tropical Pacific Ocean.

El Niño is associated with the weakening of easterly trade winds and the movement of warm water from the western Pacific toward the western coast of the Americas. The phenomenon can have widespread effects, often bringing cooler, wetter conditions to the U.S. Southwest and drought to countries in the western Pacific, such as Indonesia and Australia.

Satellite and ocean-based measurements of sea surface temperature are one way to detect the arrival of El Niño. Its signature also shows up in satellite measurements of sea surface height, which rises as ocean temperatures warm up. That's because warmer water expands to fill more volume, while cooler water contracts.

The map above depicts sea surface height anomalies across the central and eastern Pacific Ocean as observed from June 1–10, 2023. Shades of blue indicate sea levels that were lower than average, normal sea level conditions appear white and reds indicate areas where the ocean stood higher than normal.

Data for the map were acquired by the *Sentinel-6 Michael Freilich* and *Sentinel-3B* satellites and processed by scientists at NASA's Jet Propulsion Laboratory (JPL). Note that signals related to seasonal cycles and long-term trends have been removed to highlight sea level anomalies associated with El Niño and other short-term natural phenomena.

In a report released on June 8, 2023, the *NOAA Climate Prediction Center* declared El Niño conditions to be present. The report pointed to sea surface temperatures in the Niño 3.4 region of the tropical Pacific (between 170° to 120° west longitude) that in May 2023 were 0.8°C above the long-term average.

Forecasters expected El Niño conditions to gradually strengthen into the 2023–2024 Northern Hemisphere winter, by which time they called for a 60% chance of a moderate strength El Niño developing and a 56% chance of a strong El Niño.

As of June 2023, however, El Niño was not as far developed as past El Niño events by the same time of year, according to Josh Willis, an oceanographer and Sentinel-6 Michael Freilich project scientist at JPL.

"*It's still a bit too early to say whether this will be a big one*," Willis said. "*It will probably have some global impacts, but there's still time for this El Niño to underwhelm.*"

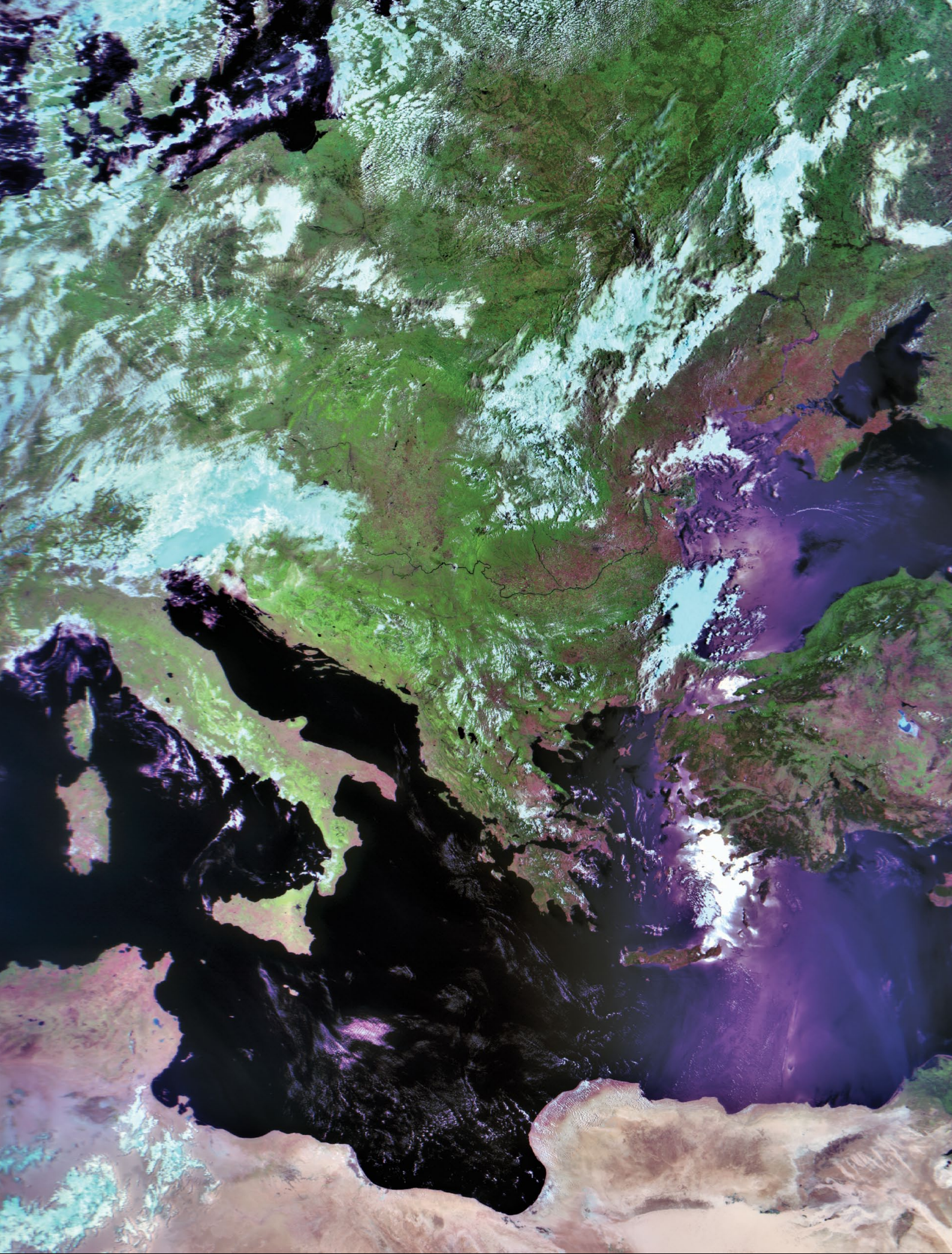

This is a section from an RGB123 image received from the HRPT transmission of the newly orbited Meteor MN 2-3 satellite at 07.50 UT on July 3, 2023 by Enrico Gobbetti. Note the fine detail of the Rivers Danube and Dnipro as they course towards the Black Sea.

The Cascades Range in Washington and Oregon

MODIS Web Image of the Day

Image Credit: MODIS Land Rapid Response Team, NASA GSFC

The Cascade Range, stretching 1,300 kilometres from northern California, U.S.A, to southern British Columbia, Canada, separates the moist, green coastal plain from the dry interior landscape. The peaks of the Cascades are actually a volcanic chain created by the slow movement of dense oceanic crust as it slides beneath North America.

The mountains contain towering volcanic peaks, many of which are currently considered active even though eruptions in recorded history have been rare. The most recent was the eruption of Mount St. Helens on May 18, 1980. Because of the risk that eruptions could present to human life and property, the United States Geological Survey (USGS) Cascades Volcano Observatory (CVO) monitors ten volcanoes in the Cascades. Five of these are in Washington (Glacier Peak, Mount Adams, Mount Baker, Mount Rainier, and Mount St. Helens), while the remainder are in Oregon (Mount Hood, Mount Jefferson, Newberry, Three Sisters, and Crater Lake).

Oh June 4, 2023, the Moderate Resolution Imaging Spectroradiometer (MODIS) on board NASA's Aqua satellite acquired a true-colour image of the Cascades Range in part of the states of Washington (north) and Oregon (south).

The boundary line between the states runs along the Columbia River, which flows from inland, westward to the Pacific Ocean through a deep gorge between the mountains. Snow caps the tallest volcanic peaks, while lower elevations are green with summer vegetations.

The snow-capped volcanoes in this image are, from north to south, Mount Rainier, Mount St. Helens (west), Mount Adams (east), Mount Hood, and Mount Jefferson. Snow also sits atop the Goat Rocks Wilderness, located between Mount Rainer and Mount Adams. The Goat Rocks are remnants of a large volcano, extinct for about two million years.

Canadian Smoke Reaches Europe

NASA Earth Observatory

Story by Kathryn Hansen

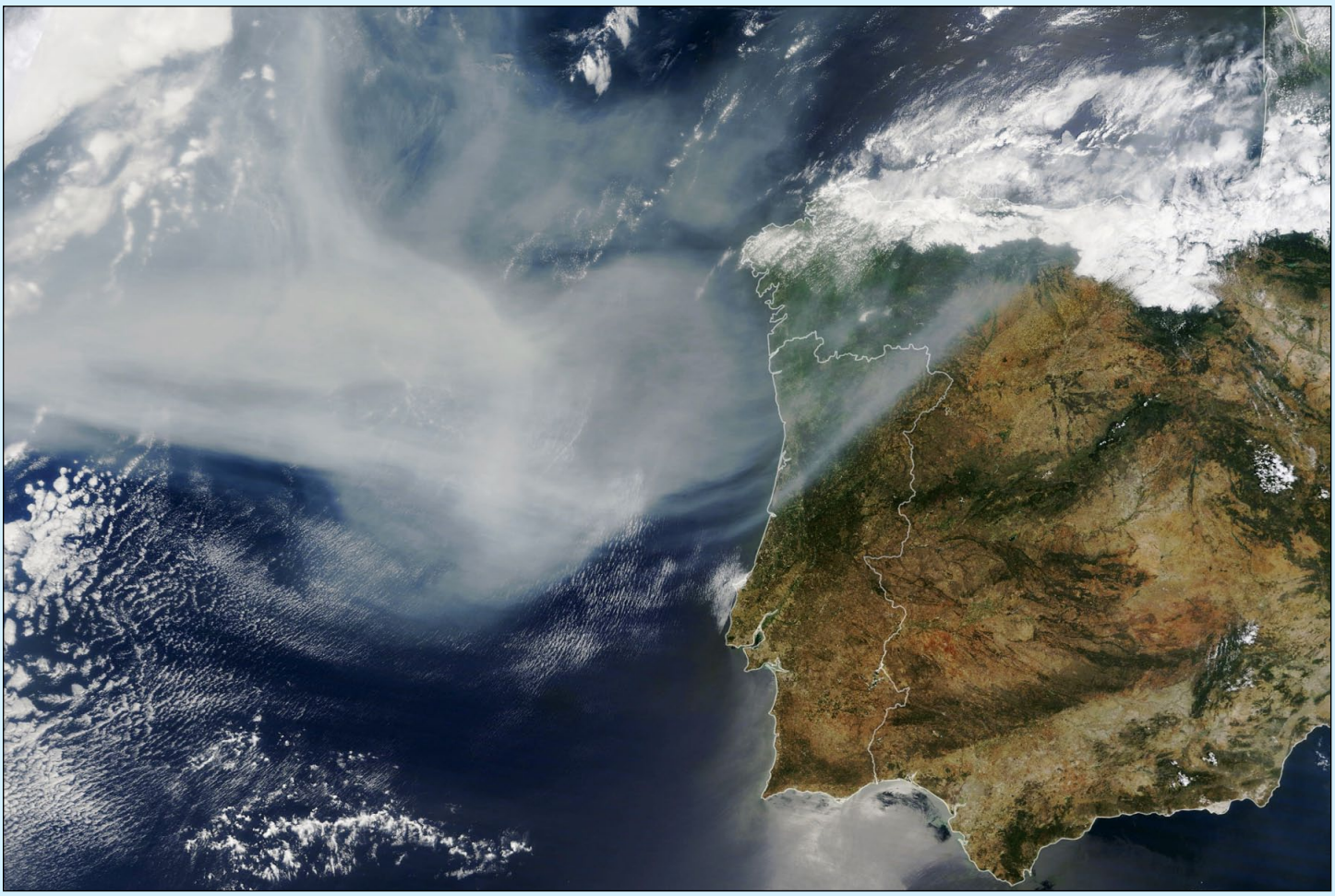

Figure 1 - This MODIS image from NASA's Terra satellite shows smoke from Canada drifting over Portugal and Spain.
NASA Earth Observatory image by Lauren Dauphin, using MODIS data from NASA EOSDIS LANCE and GIBS/Worldview

Smoke from wildland fires, which had been burning in the Canadian province of Quebec for weeks, eventually crossed the Atlantic Ocean and darkened skies over southwestern Europe.

The Moderate Resolution Imaging Spectroradiometer (MODIS) on NASA's Terra satellite acquired figure 1 in the morning (11:10 Universal Time) of June 26, 2023. At that time, smoke was drifting over northern Portugal and Spain. The smoke also reached northward over other European countries beyond the scope of this image.

The smoke's widespread reach is apparent in the map opposite (figure2). It shows a plume of black carbon particles—commonly called soot—spanning eastward from North America and across more than 2,000 miles of the Atlantic Ocean. The black carbon density data come from NASA's GEOS forward processing (GEOS-FP) model,

https://gmao.gsfc.nasa.gov/GMAO_products/

which assimilates data from satellite, aircraft, and ground-based observing systems. In addition to

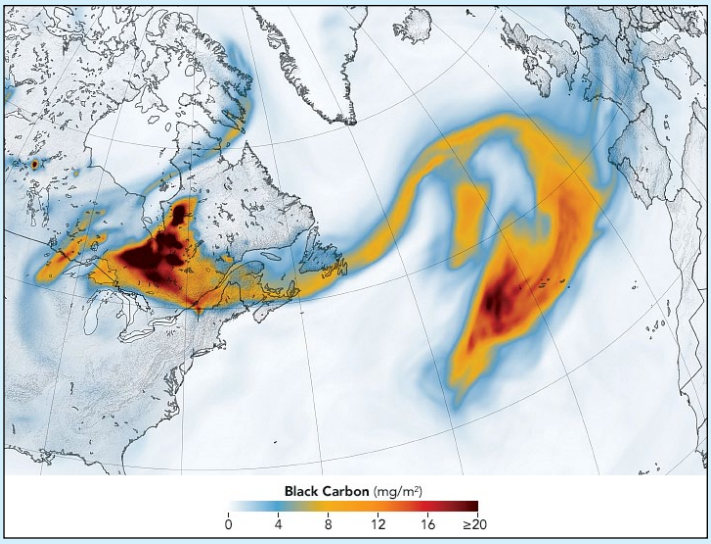

Figure 2
A Map showing the track of the smoke across the Atlantic Ocean during June 2023
NASA Earth Observatory images by Lauren Dauphin, using MODIS data from NASA EOSDIS LANCE and GIBS/Worldview and GEOS-5 data from the Global Modelling and Assimilation Office at NASA GSFC.

making use of satellite observations of aerosols and fires, GEOS-FP incorporates meteorological data like air temperature, moisture, and winds to project the plume's behaviour.

Hazy skies in Europe were also observed by a global network of ground sensors called the Aerosols Robotic Network, or AERONET. The network contains more than 500 Sun photometer instruments that measure aerosol optical depth (AOD) around the world. On the morning of June 26, AERONET sensors in northern Spain and France measured AODs greater than 0.5. The AOD in these areas is typically close to 0.1. (For reference, a perfectly clear sky would have an AOD of less than 0.05, while an AOD of 3 would make it difficult to see the Sun.)

Yet air quality in the smoke-covered parts of Europe on June 26 remained mostly fair, compared to unhealthy and hazardous air quality in the smoke-affected parts of Canada and the United States. That's because most of the smoke that reached Europe was higher in the atmosphere, where it is less likely to affect human health.

The smoke over Europe will probably be noticed by people. According to the UK Met Office, the smoke aerosols could contribute to vivid sunrises and sunsets.

Climate Change threatens glaciers in the Himalayas

Copernicus Image of the Day

Credit: European Union, Copernicus Sentinel-2 imagery

The Karakoram range in the Himalayas is renowned for its glaciers, some of which are among the largest and longest outside the polar regions.

As a result of climate change, these glaciers are melting at an accelerated rate, leading to the formation of new glacial lakes in the Hunza River basin and in other valleys of the range, as seen in this Copernicus Sentinel-2 image of 15 April 2023.

A recent article published in the Nature scientific journal highlights the critical dependency of the Hunza River basin on frozen water resources and warns that future changes in the hydrological regime in this area could have serious consequences for the water flow of the Indus River.

Copernicus provides satellite data and services that enable the monitoring of glaciers, including their size, shape, and movement over time.

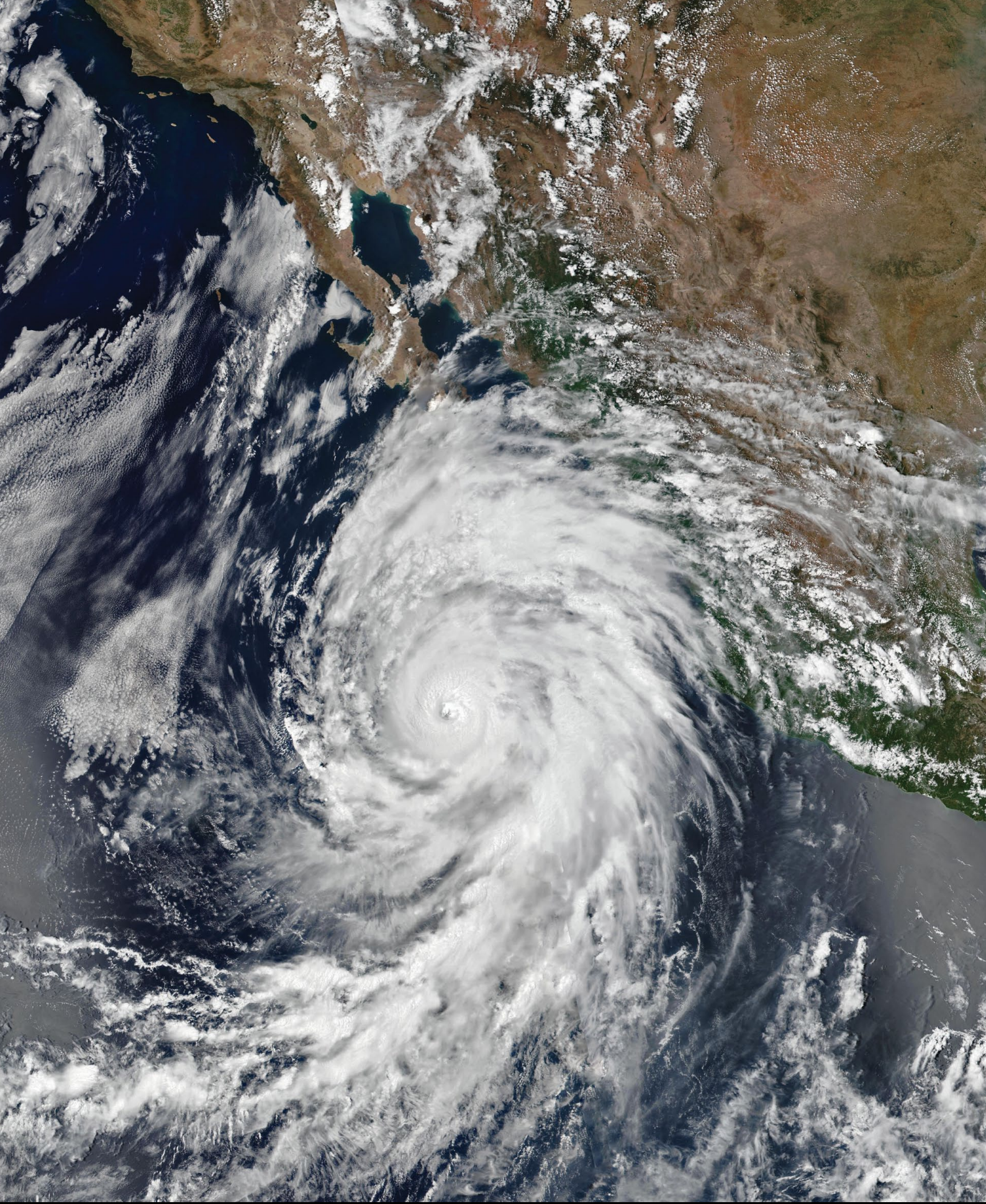

NASA's Suomi-NPP satellite captured this image of category-4 Pacific Hurricane Hilary as it approached California on August 18, 2023. Two days later Hilary became the first tropical storm to make landfall in the south of California for 84 years, causing flooding, mudslides, and power outages in its wake. Bringing 110 kph wind gusts that downed trees and power lines, the storm produced the wettest August day on record for both Los Angeles and San Diego with 6.3 centimetres and 4.6 centimeters of rain, respectively. Streets turned into rivers of mud in Palm Springs after the city received six months of rain over six hours. Some of the most severely affected places were the normally dry desert regions of Southern California, and Death Valley received 5.6 centimetres of rainfall, equivalent to it's total mean annual precipitation, in just 24 hours.

La Palma on Fire

NASA Earth Observatory

Story by Adam Voiland

In the early hours of July 15, 2023, a wildfire broke out on La Palma, the most northwesterly of the Canary Islands. The Moderate Resolution Imaging Spectroradiometer (MODIS) on NASA's Aqua satellite captured this image of smoke streaming south from the blaze that afternoon. The bright areas near islands south of La Palma resemble smoke, but they are actually the result of an optical phenomenon caused by sunglint.

The fire burned through pine forests west of a large caldera on the northern part of the island. At least 20 buildings were destroyed and 4,000 people evacuated their homes, according to Reuters. On June 16, authorities reported that the fire had charred at least 46.5 square kilometres. Hot weather and strong winds accompanied the intense burning. The same heatwave scorched parts of southern Europe and North Africa. The Associated Press reported that more favorable weather conditions on July 16 helped firefighters slow the blaze. Satellite images collected on July 16, 17, and 18 showed much less smoke coming from the fire.

Fires on La Palma are common in summer due to the island's dry climate. One analysis of tree rings suggests that intense fires burn the island's forests roughly every seven years on average, with less intense fires burning every 2-4 years.

In addition to fire, volcanic activity can also damage infrastructure and alter La Palma's landscape. A slow-moving eruption destroyed 1,600 homes on the island in the latter part of 2021.

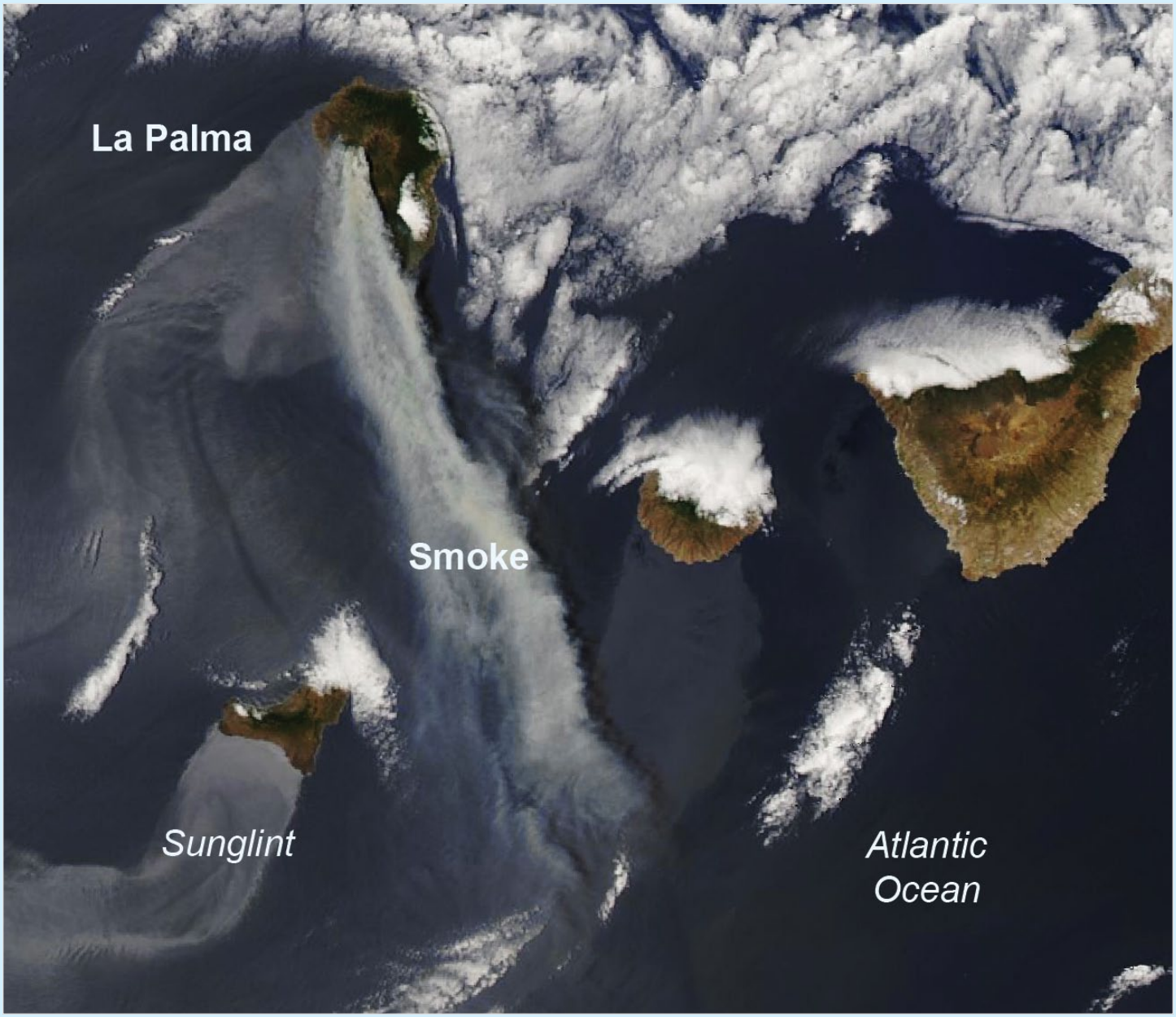

NASA Earth Observatory images by Wanmei Liang, using MODIS data from NASA EOSDIS LANCE and GIBS/Worldview.

Himarawicast Imagery of Typhoon Doksuri

David Sale

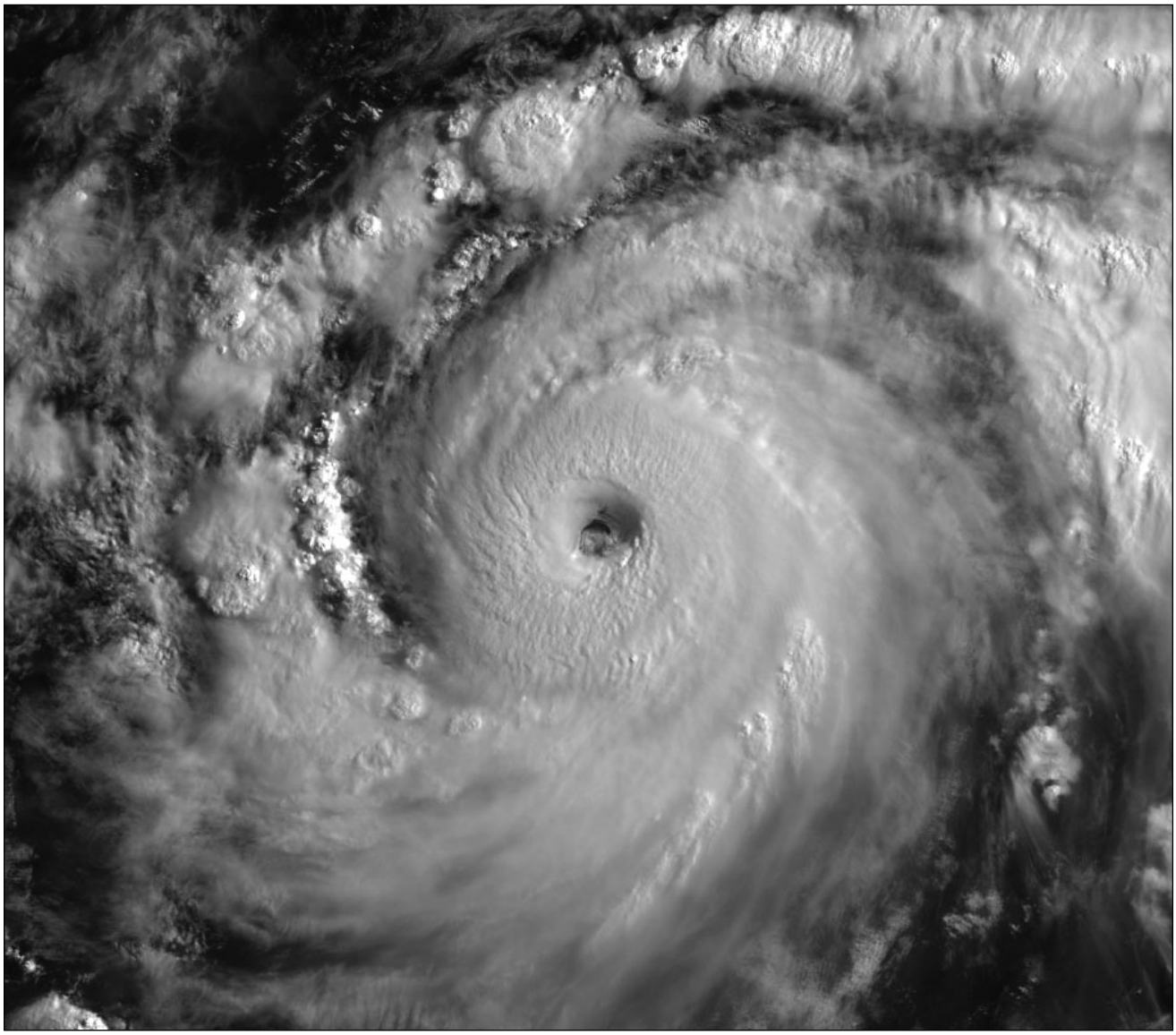

This image of Typhoon Doksuri was captured by Himawari-9 on July 24, 2003
Credit: HimawariCast

Himawaricast is a DVB-S2 C-band re-transmission of Himawari-9 data that can be received in the western Pacific region. Full disk images are sent every 10 minutes with one kilometre resolution for the visible spectrum (as in the image above), and 4 kilometres for the remaining 14 bands. Fortunately, the data is unencrypted and available to amateur users.

The image above is one that I received from Australia via Himawaricast: Typhoon Doksuri ('Eagle' in Korean) on July 24 as it was heading west towards China. The storm caused considerable flooding in the Philippines and Taiwan before wreaking havoc on the Chinese mainland.

Typhoon Doksuri proved to be the worst to hit China in over a decade, with Beijing experiencing its heaviest rainfall in 140 years. At least 20 deaths were recorded while hundreds of thousands of residents were displaced by widespread flooding and damage in a region the size of Great Britain. Beijing's Changping district recorded 744.8 millimetres of rainfall during a four day period, far exceeding the previous record of 609 mm set in 1891.

In the urban areas of Beijing, hundreds of roads were flooded, forcing parks and tourist spots to shut. Hundreds of flights were either delayed or cancelled at the city's two major airports. Some subway lines and trains were also suspended on account of flooding.

In Mentougou and Fangshan districts, raging water coursed down roads, sweeping away dozens of cars. Villages in mountainous areas were cut off, prompting authorities to deploy helicopters to drop off food, water and emergency supplies. Zhuozhou, a city with more than 600,000 inhabitants located southwest of Beijing was half-submerged and over one sixth of it's population was evacuated.
You can read much more about this Typhoon at

https://en.wikipedia.org/wiki/Typhoon_Doksuri_(2023)

Shrinking Iceberg A-76A

NASA EArth Observatory

Story by Kathryn Hansen

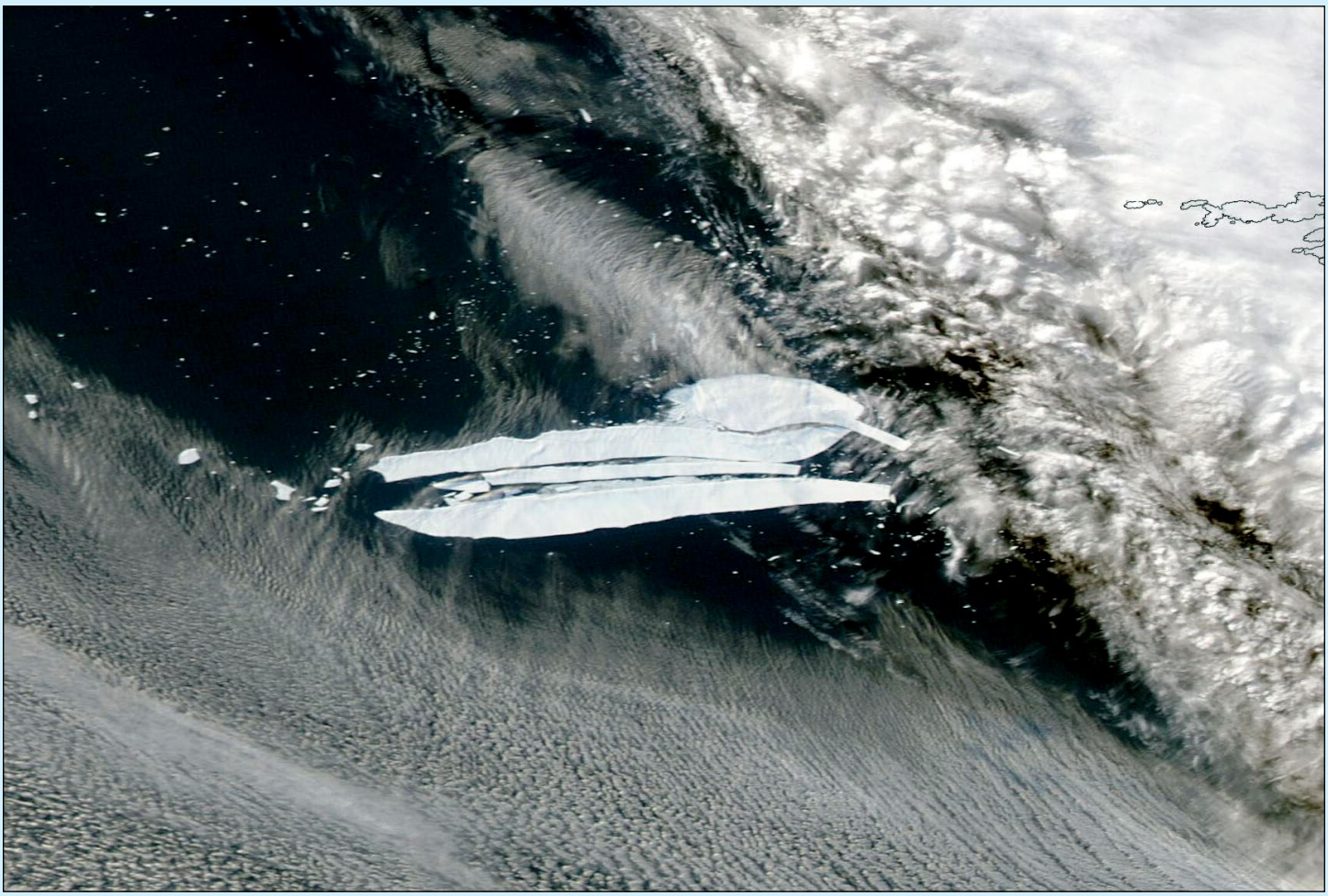

NASA Earth Observatory image by Wanmei Liang, using MODIS data from NASA EOSDIS LANCE and GIBS/Worldview

In May 2021, Iceberg A-76 broke from the Ronne Ice Shelf in Antarctica. At the time, it was the largest iceberg floating anywhere in the world. Two years later, only fragments of the former berg remain.

The Moderate Resolution Imaging Spectroradiometer (MODIS) on NASA's Terra satellite acquired this image on May 24, 2023. It shows Iceberg A-76A, which broke from A-76 shortly after the initial calving and remains the event's largest surviving berg. But its size has dwindled during the past month as pieces have splintered off in warmer, more northern waters.

At the time of this image, Iceberg A-76A and several newly separated pieces floated near the remote island of South Georgia. They were about 2,400 kilometres north of the berg's origin near the Ronne Ice Shelf.

'*It is impressive to think it 'sailed' that far in about two years*,' said Christopher Shuman, a University of Maryland, Baltimore County, glaciologist based at NASA's Goddard Space Flight Center. '*That obviously speaks to the force of powerful currents in this part of the Southern Ocean.*'

By October 2022, Iceberg A-76A had most likely escaped the clockwise circulation of the Weddell Gyre and entered the Drake Passage—the turbulent body of water between South America's Cape Horn and Antarctica's South Shetland Islands. More than a year into its voyage, the berg's size had not changed much. It still measured 135 kilometres long and 26 kilometers wide—a total area about twice the size of London.

But the Drake Passage often marks a turning point for icebergs. From there, they typically whip north toward the South Atlantic and quickly melt in the region's warmer—but still chilly—waters. Iceberg A-76A appears to be experiencing this same fate as it nears South Georgia late in the austral autumn. Around the time of this image, A-76A measured 78 kilometres long and 11 kilometers wide—an area about the size of Austin, Texas.

Other major icebergs have met their demise in a similar fashion. Notably, the Delaware-sized Iceberg A-68A that broke from Antarctica's Larsen C Ice Shelf in July 2017, and which finally splintered apart in the waters around South Georgia in February 2021.

Canals in Ukraine are Drying Up

A NASA Earth Observatory Feature

Story by Adam Voiland

When the Kakhovka Dam was breached on June 6, 2023, water from the adjacent reservoir surged into the Dnipro River toward the city of Kherson and the Black Sea, causing severe flooding downstream. Floodwaters began to recede after a few weeks, but a slower-moving water problem has unfolded in southern Ukraine as networks of canals once fed by the Kakhovka Reservoir run dry.

Scientists with *NASA's Harvest Consortium* have been monitoring the situation closely, with a focus on determining how the event is affecting farmers. The research is part of a broader effort to develop analytical tools, based on satellite observations, to quickly assess how crop conditions and the war in Ukraine are affecting global food supplies.

'*The major challenge for farmers now is lack of water*,' said Inbal Becker-Reshef, NASA Harvest's director. '*Networks of canals that are normally fed by the Kakhovka Reservoir have become disconnected from the reservoir and are drying out.*'

Analysis by *NASA Harvest* shows that all four of the major inlets that supply the canal networks have been disconnected. While abundant rainfall in spring and early summer prevented the canals from going completely dry (figure 1), satellite observations show a narrowing of the canals suggesting large reductions in the amount of water (figure 2).

The Ministry of Agrarian Policy and Food of Ukraine noted that the loss of water for hundreds of thousands of hectares could turn farmland in this area into 'deserts' by 2024. The lack of irrigation could also have ripple effects that cause farmers to produce fewer crops on non-irrigated fields due to loss of income, according to the ministry. 'A *million and a half hectares will not be used to their full potential*,' stated Mykola Solskyi, Ukraine's minister of agrarian policy.

Figure 1 - Kakhovka Reservoir and canals on May 17, 2023

Figure 2 - Kakhovka Reservoir and canals on June 18, 2023

Inlets to the North Crimean Canal and the Kakhovsky Canal—two of the four major canal networks fed by the Kakhovka Reservoir—are visible in the images above.

Figure 3 - These images show a closer view of changes at the inlet of the NorthCrimean Canal
Planet Labs images courtesy of Inbal Becker-Reshef.

Figure 1 shows the inlets on May 17, 2023, when they were full of water. Figure 2 shows the same canals on June 18, after water levels in the reservoir had dropped below what is required for water to enter the canals. Both images were acquired with the Operational Land Imager-2 (OLI-2) on Landsat 9. (Note that the apparent browning in the centre-pivot fields is due to the normal harvest cycle, not lack of water. As winter wheat and other crops are harvested and tilled, the fields appear brown before the next crop is planted.)

The pair of images at the top of this page (figure 3), from *Planet Labs*, shows a closer view of changes at the inlet of the North Crimean Canal. The left image shows the canal on June 3, 2023. The second image shows the same area on July 19, 2023, as the inlet and canal were drying up.

'*Many of the summer crops grown in Kherson—such as corn, wheat, sunflower, tomatoes, and melons—are heavily reliant on irrigation, and summer rains are unlikely to be sufficient to maintain crop health and average yields of irrigated crops*,' said Becker-Reshef.

Figure 4 - Kakhovka reservoir before and after the flood

The reason for the irrigation challenges is apparent in the pair of satellite images in Figure 4. After the dam breach, the reservoir that once sustained the canals mostly emptied, exposing broad expanses of mud. The upper image was acquired by Landsat 8 on June 7, 2022, about one year before the dam

Figure 5 - The flooded Dnipro River on June 9, 2023

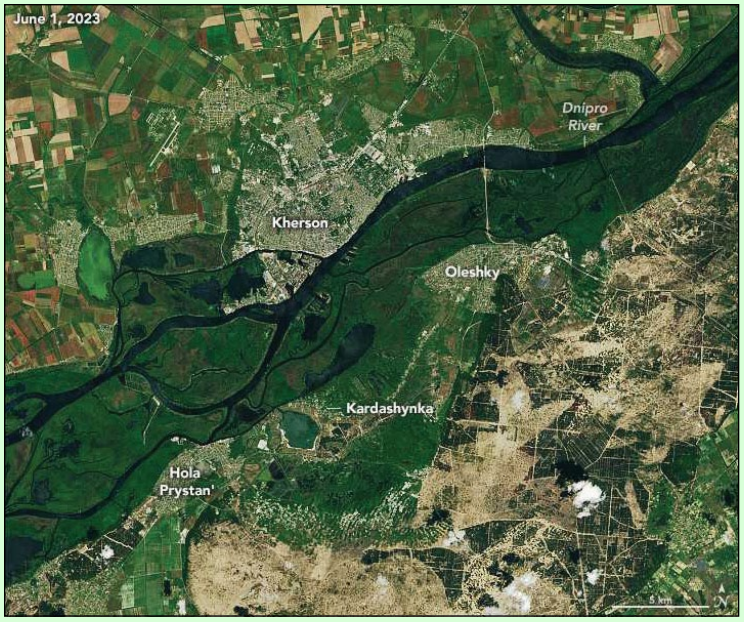

Figure 6 - The Dnipro River on June 1, 2023, before the flood

was damaged. The lower image, acquired by OLI-2 on Landsat 9, shows the same area this June 18, after roughly 75% of the water in the reservoir had drained—a volume of water roughly equivalent to Utah's Great Salt Lake.

Satellite altimetry data provided by the *U.S. Foreign Agriculture Service* and the French data services centre (*Theia*) confirmed that water levels dropped by several metres over a few days soon after the dam failed. This came after water levels had climbed to a 30-year high following a wet spring.

Figure 5 shows flooding along the Dnipro River near the city of Kherson on June 9, 2023, three days after the dam was breached, as acquired by the OLI-2 on Landsat 9. For comparison, figure 6 shows the same area on June 1, 2023, acquired by the OLI aboard Landsat 8. The most severe flooding was on the east side of the river, which is at an overall lower elevation and more flood prone than the west side. During the worst of the flooding, several thousand homes were inundated, tens of thousands of people lost power, and more than 40,000 were forced to evacuate.

The *NASA Harvest Team*—in partnership with *Sertit* (University of Strasbourg)—used Planet and Sentinel-3 data to produce a comprehensive map of flooded croplands, flooded villages, and open water that they provided to the Ukrainian Ministry of Agriculture as part of the humanitarian response efforts following the dam breach.

They also continue to monitor the main canal inlets from the Kakhovka Reservoir and are developing methods to use satellites to track how much irrigation water fields receive throughout the summer.

NASA Harvest analysts will also be monitoring the health of crops using tools such as the GIMMS Global Agricultural Monitoring tool and the AGMET EO Indicator dashboard. These tools had not yet shown a major drop in the greenness of crops by early July 2023 due to regular rains, though the loss of irrigation water could begin to brown these crops in the future.

The semi-arid steppe ecosystems found in the Kherson, Zaporizhzhia, and Dnipropetrovsk oblasts generally receive 100 to 120 millimetres of rain during the summer growing season—not typically enough for some crops to thrive without irrigation. More than 12,000 kilometres of canals constructed since the 1960s have provided irrigation water for up to 500,000 hectares (5,000 square kilometres) of croplands, turning the region into one of the most productive farming regions in Ukraine. Canal water is also used for drinking water, industry, and other public uses.

The *Ukrainian Grain Council* has estimated that the flood could lead to a 14% reduction in the volume of Ukraine's grain exports. In late June 2023, *NASA Harvest* estimated that Ukraine would produce 25 million tons of wheat this year, about two million tons lower than the five-year average. *NASA Harvest* will continue to monitor the situation in the coming months and will post updates in its news feed.

NASA Earth Observatory images in this article by Lauren Dauphin using Landsat data from the U.S. Geological Survey

Large Phytoplankton Bloom in the Barents Sea

Copernicus Image of the Day

https://www.copernicus.eu/en/media/image-day

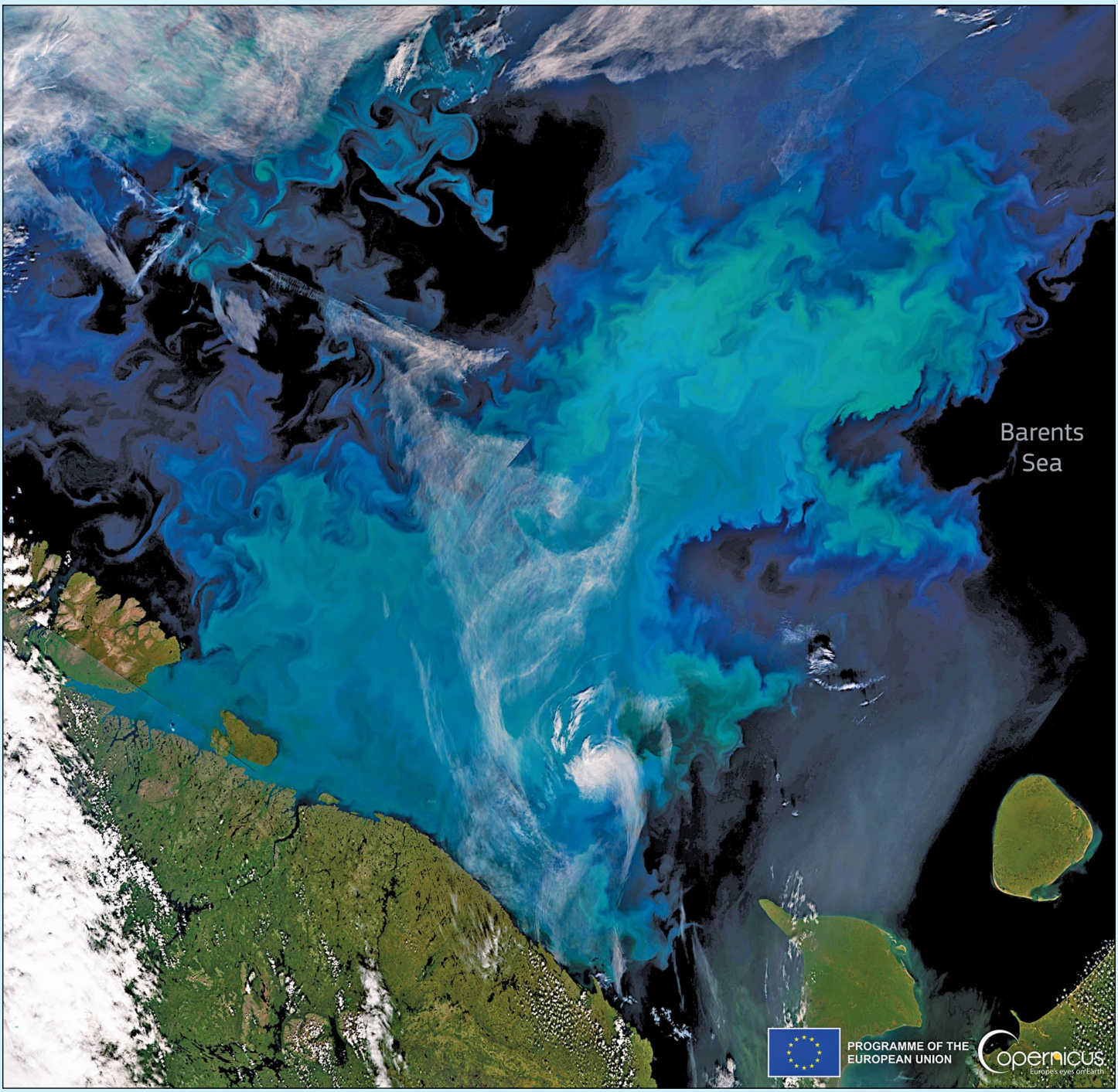

Credit: European Union, Copernicus Sentinel-3 imagery

This image, acquired by one of the Copernicus Sentinel-3 satellites on August 3, 2023, shows a large phytoplankton bloom north of the Scandinavian Peninsula, spanning over 200,000 square kilometres.

Phytoplankton consists of microscopic plant-like organisms that float in seas and oceans, and which play a vital role in the marine ecosystem. In the Barents Sea, an Arctic region subject to a delicate equilibrium between temperature and salinity, these blooms are a relatively common phenomenon, particularly during the summer months when the abundance of sunlight stimulates phytoplankton growth.

Observation of these phenomena is crucial for understanding changes in marine ecosystems and potential repercussions on fish resources and global climate. Copernicus open data allow for monitoring and analysing these phenomena in near real-time.

Ebb and Flow in the Chausey Islands

NASA Earth Observatory

Story by Lindsey Doermann

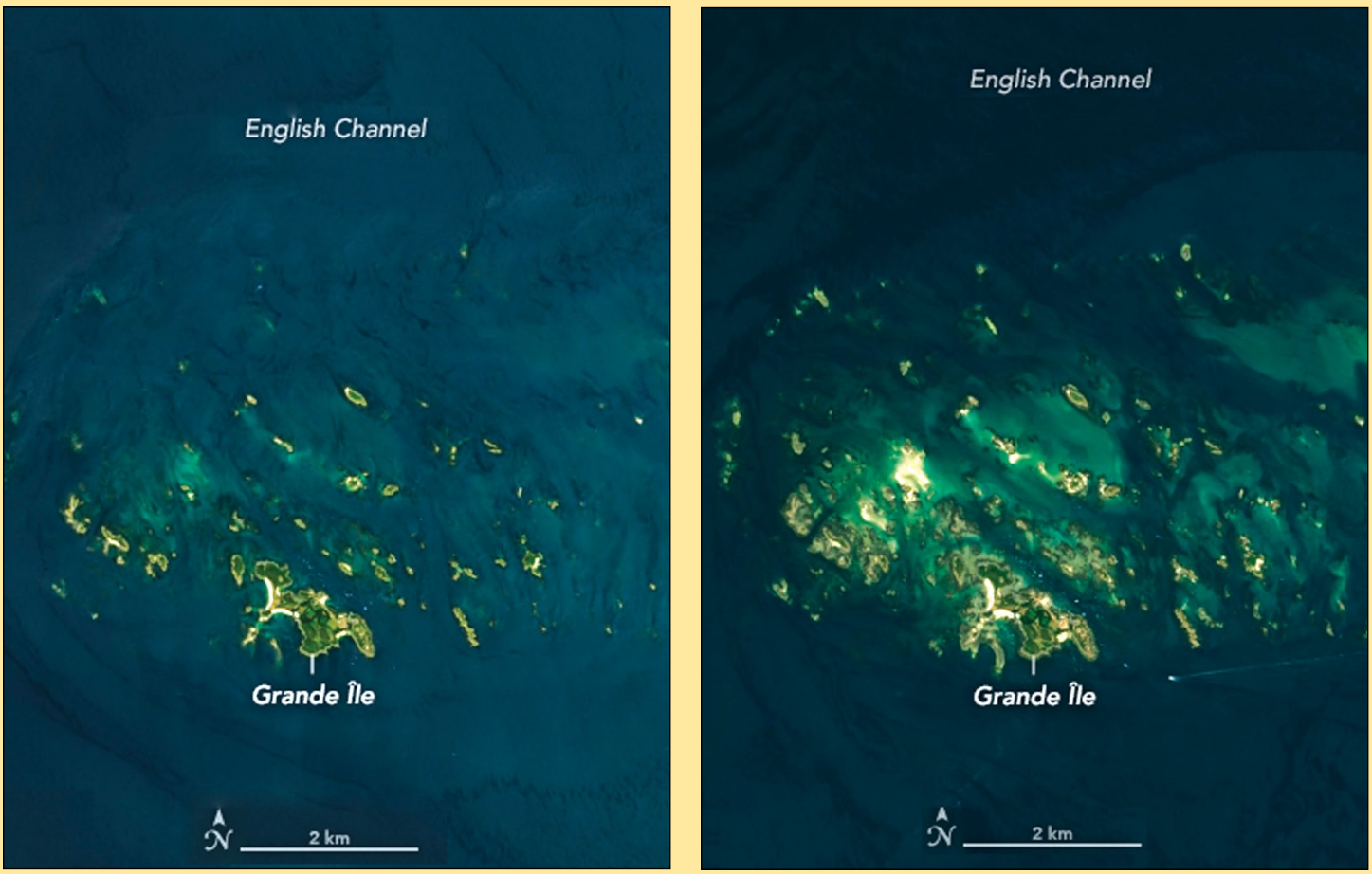

France's Chausey Islands at high tide (left) and low tide (right)
NASA Earth Observatory images by Allison Nussbaum, using Landsat data from the U.S. Geological Survey

France's Chausey Islands—Les Îles Chausey—located in the English Channel, are subject to some of the largest tidal ranges on Earth. As a result, when tides are low, the islands number 365; when tides are high, only 52 remain above water.

These images show the archipelago at opposite tidal extremes: a low-tide view from July 22, 2018 (left), and a high-tide view from April 19, 2019 (right). Both images were acquired by the Operational Land Imager (OLI) on the Landsat 8 satellite.

Chausey lies approximately 18 kilometres off the coast of Normandy. The only inhabited island in the group is Grande Île, which is reachable via a short ferry ride. At low tide, it is possible to walk between some of the granite isles on sandy tidal flats. The area provides habitat for abundant seabirds and marine life and is protected as a European Environment Agency Natura 2000 site.

While the planet's most extreme tidal swings are found across the Atlantic Ocean, in Canada's Bay of Fundy, where they can reach a maximum of some 16 metres, the tidal swings at Chausey still rank among the world's largest. While the mean tidal range at the islands is 8.2 metres, during a spring tide it can exceed 14 metres .

Many factors, including the shape of coastlines, size of the ocean basin, and position of the Sun and Moon, govern the height of tides. At higher latitudes in the northern hemisphere, the relative closeness of the continents plays a large role in producing greater tidal ranges in the way it effectively constricts the oceans.

The English Channel's energetic tides have been considered for tidal power schemes dating back to at least the 1960s. While no tidal generators were ever installed at the Chausey Islands, the world's first tidal power plant in the nearby estuary of the Rance River came online in 1966 and continues to generate electricity today. With a capacity of 240 megawatts, it was the largest operating tidal power plant in the world until the Sihwa Lake Tidal Power Station in South Korea opened in 2011.

Wildfire in Portugal

Copernicus Image of the Day

https://www.copernicus.eu/en/media/image-day

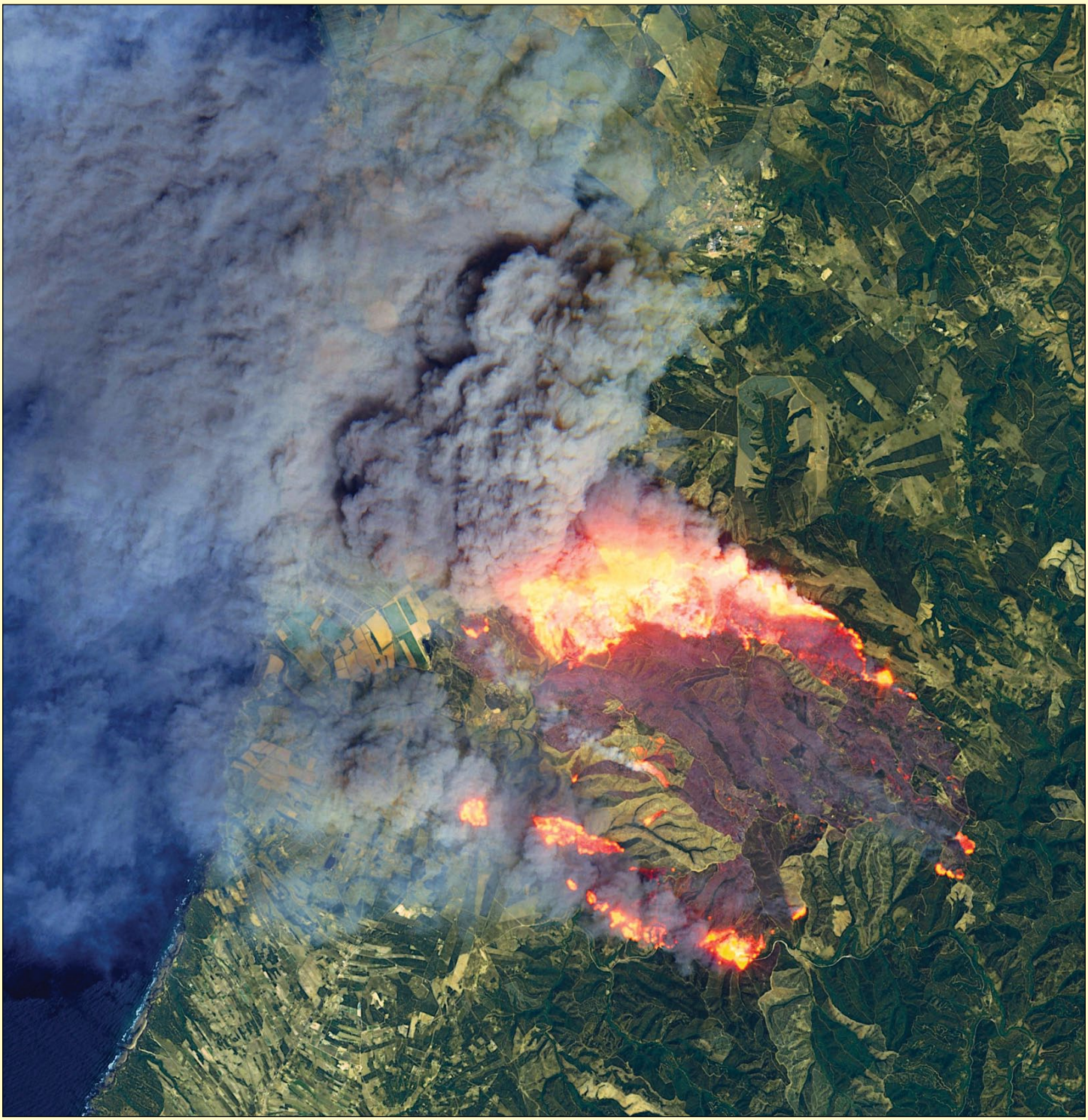

Credit: European Union, Copernicus Sentinel-3 imagery

On 5 August, a blaze erupted near Odemira, in the Alentejo region, prompting a massive response with more than 800 firefighters and 202 vehicles to control the flames. The severity of the fire resulted in the evacuation of four communities in Odemira (Vale dos Alhos, Vale de Água, Choça dos Vales, and Relva Grande) and a rural tourism area. The fire also encroached upon two protected areas, the Parque Natural do Sudoeste Alentejano e Costa Vicentina and Zonas de Protecção Especial de Monchique, putting unique ecosystems and wildlife at significant risk.

This image, captured by one of the Copernicus Sentinel-2 satellites on 7 August, shows the hotspots and the massive smoke cloud generated by the wildfire reaching the Atlantic Ocean.

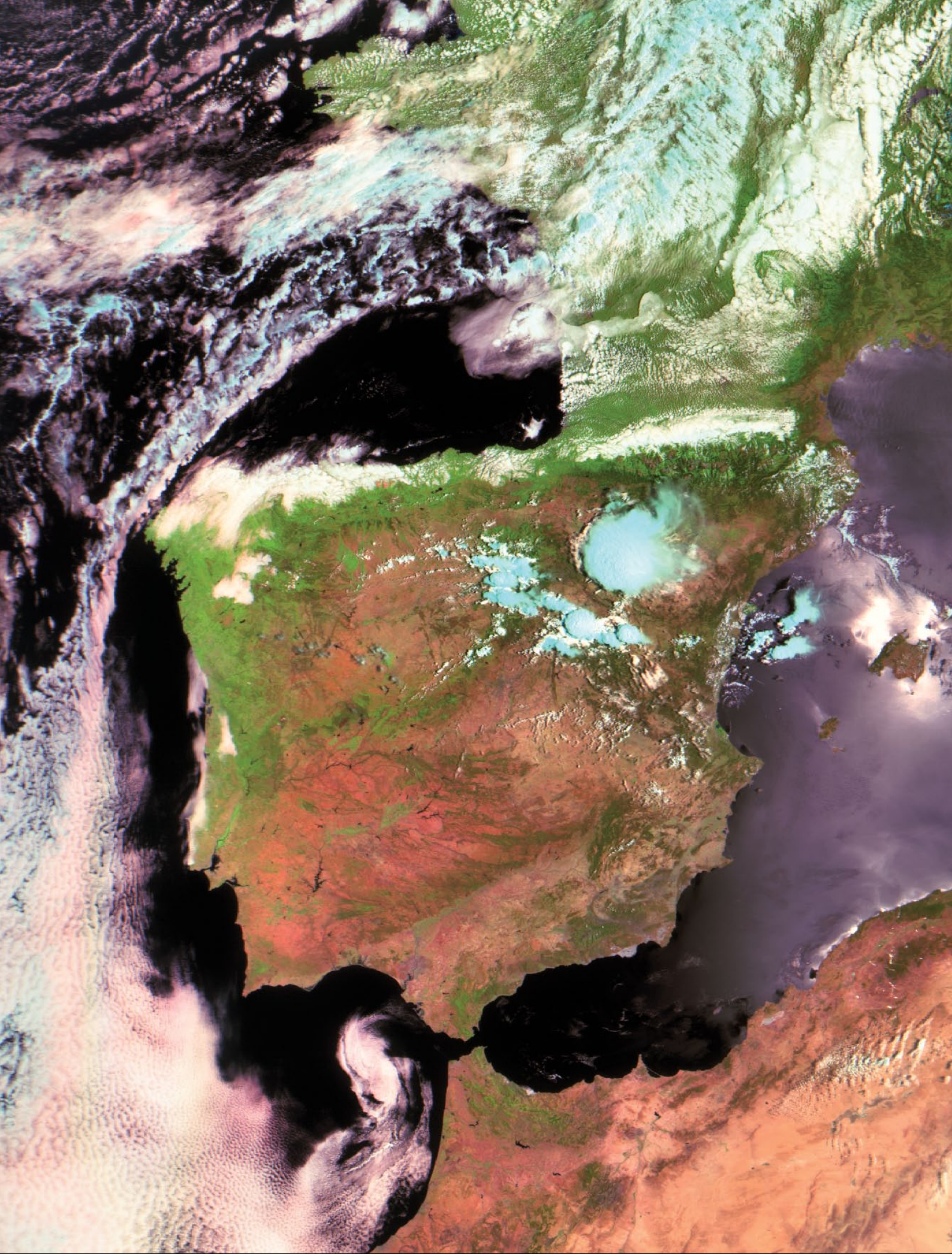

This segment from an RGB123 image received from the HRPT transmission of the newly orbited Meteor MN 2-3 satellite at 09.31 UT on July 3, 2023 by Enrico Gobbetti provides a striking rendition of Spain and the Strait of Gibraltar.

Joachim Scharrer submitted this Meteor M 2-3 channel-4 infrared image clearly showing Italy, on August 10, 2023.

Cook Strait, New Zealand

European Space Agency

Image contains modified Copernicus Sentinel data (2021), processed by ESA, CC BY-SA 3.0 IGO

The Copernicus Sentinel-2 mission takes us over Cook Strait, which separates New Zealand's North and South Islands.

Named after James Cook, who was the first European to sail through it, the Cook Strait is just 23 kilometres wide at its narrowest point so, on a clear day, it is possible to see across the strait. However, it is also renowned as one of the roughest and most unpredictable stretches of water in the world, owing to strong winds, conflicting currents and variable tides.

This dynamic environment is depicted here by the various shades of blue in the water and swirls. Both shores feature steep cliffs which, in the image, result in the white colour caused by the big waves crashing against the rocky coast.

New Zealand comprises many islands, though the North and South Islands are the largest. North Island, visible on the right, is home to Wellington, New Zealand's capital city, which lies on the hills and shore around the bay in the extreme south of the island.

South Island is connected to North Island by a ferry service from Wellington to Picton, a port town near the head of Queen Charlotte Sound. The sound is a deep inlet visible in dark blue in the upper part of South Island. Numerous ferries can be spotted as white dots in the sound.

Moving south, a patchwork of agricultural fields cover the Wairau Plain and surround the town of Blenheim, visible in grey.

Several rivers cross the plain. The biggest in the image, the Wairau River, is one of the longest in New Zealand. It can be seen meandering through the fields and splitting into separate arms which eventually enter Cloudy Bay in Cook Strait. The southernmost arm of the river forms an estuary, which feeds a network of ponds, marshes and lagoons, sheltered from the Pacific Ocean by an eight kilometre long boulder bank.

Cloud Streets over the Labrador Sea

MODIS Web Image of the Day

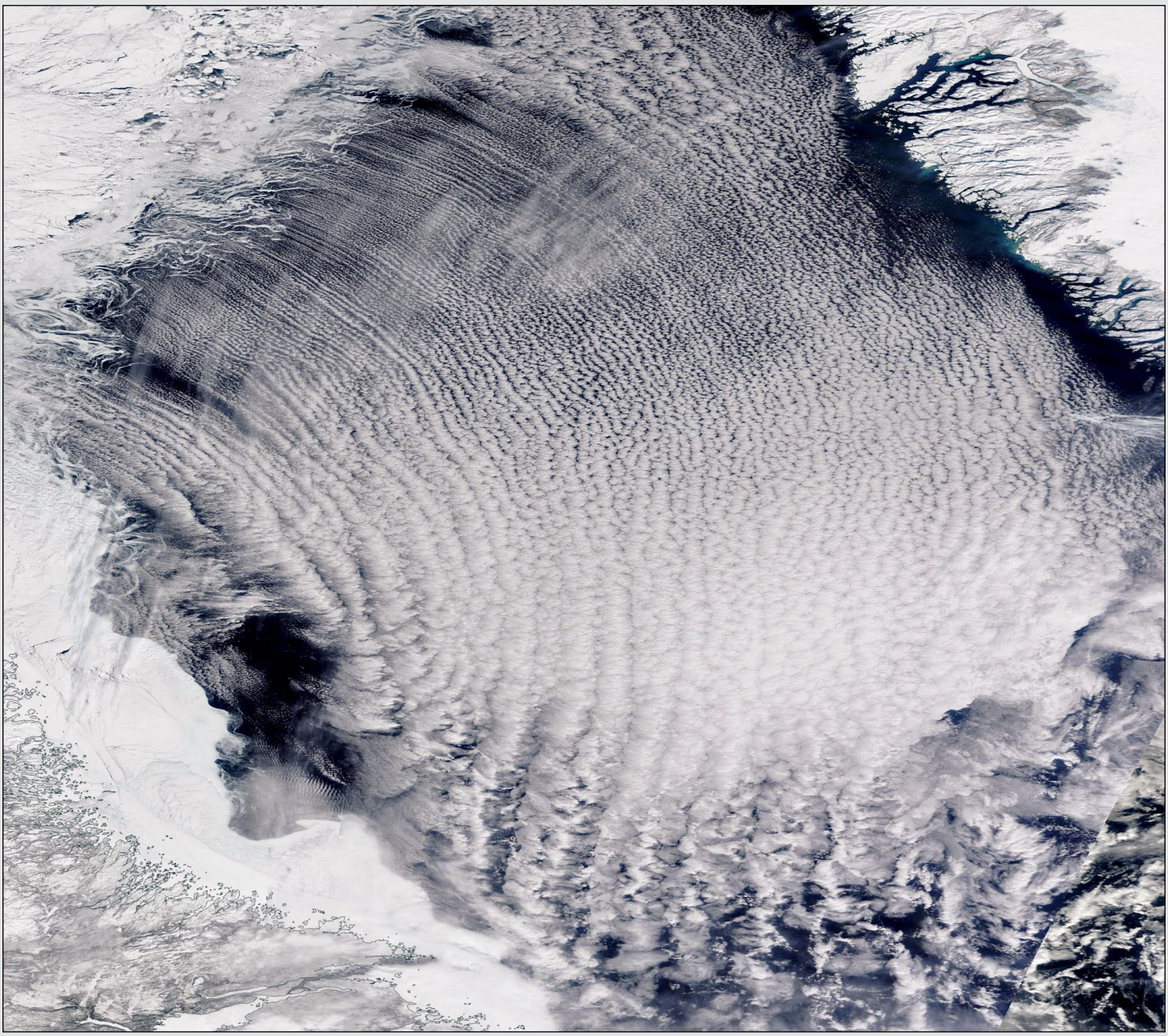

Image Credit: MODIS Land Rapid Response Team, NASA GSFC

On March 23, 2023, the Moderate Resolution Imaging Spectroradiometer (MODIS) on board NASA's Terra satellite captured yhis true-color image of a spectacular cloud formation above the Labrador Sea.

The Labrador Sea is flanked by Canada's Labrador Peninsula in the southwest and Greenland in the northeast. It is part of the North Atlantic Ocean and connects to the Arctic Ocean via various straits and bays to the north. Springtime brings big changes to the region, as fast ice—ice which clings to shore—and floating sea ice begin to melt as daylight lengthens. Despite warming air temperature, strong winds often blow from the north, carrying bitterly frigid air. Both the melting ice and frigid air can create beautiful patterns when viewed from space.

In this image, the sheets of fast ice clinging to the Labrador Peninsula are edged with delicate filigrees. These delicate patterns are created by the interaction of thin ice floating over moving currents and waves.

The predominant pattern, however, is the long, parallel bands of white that stretch across the Labrador Sea. Called '*cloud streets*', this type of cumulus cloud is common during the spring, when cold, dry air blows over comparatively warmer water. The clouds form at the top of parallel cylinders of rotating air, created by rising warm, moist air. On the upward side of the cylinders (rising air), water vapour condenses and forms clouds. Along the downward side (descending air), skies remain clear. The streets form along the direction of the prevailing wind.

Experiments with EUMETCast BUFR Data

Richard Osborne

Background

The EUMETCast-Europe datastream provides files in many different formats. According to the *Product Navigator* [1], there are in excess of thirty different types. Why there are so many I have no idea but the most common types as noted by EUMETSAT on their formats webpage [2] include netCDF, HDF, BUFR and GRIB.

In edition 72 of the GEO Newsletter, I described various ways to visualise EUMETCast SAF products and established that the four formats listed above are those used across the multiple SAF providers. However, whereas there is a choice of viewers for netCDF, HDF and GRIB files that can be classified as ready to use 'out of the box' (I am not including those which require the user to run a script), BUFR files appear to be poorly served. I know of only two viewers for BUFR that fall into this category and this is despite the fact that BUFR is the second most common format after netCDF on EUMETCast-Europe according to the *Product Navigator*.

1 *BUFRdisplay* produced by Francis Breame which is a generic *BUFR Viewer* displaying data over country outlines

2 *BUFR Viewer* produced by David Taylor which is dedicated to generating a vector display over country outlines for wind products which have both a speed and a direction.

I wished to use *BUFR Viewer* to visualise the *Polar Winds* products that are derived from the METOP series of polar orbiters, but was unable to this. There was a problem as EUMETSAT had altered the format subtly and had not updated their documentation. Somewhat annoyed with this, I resolved to find a method that would allow the *BUFR Viewer* to interpret the BUFR data correctly and so began a period of research.

What is the BUFR Format?

BUFR is short for Binary Universal Form for the Representation of meteorological data. It is stored as a continuous bit-stream that does not depend on any particular hardware or software but it does depend on the availability of external data tables to fully decode the data.

I think that it is a complicated format and Francis is forthright in his dislike of BUFR, commenting on its perceived drawbacks. As a result, I am not describing the detailed format and refer the reader to external sources which may be found on an internet search for BUFR. The user guides produced by Francis on the website [3] provide a good introduction.

Looking at the *Product Navigator* for EUMETCast-Europe, products encoded with the BUFR format tend to fall into the following categories although this is not exhaustive:

1 Wind data derived from active radar scatterometers and cloud motion images

2 Soil moisture derived from active radar scatterometers

3 Atmospheric temperature and humidity profiles and trace gases derived from microwave and infrared sounders

Visualising Buffer Data

Because a BUFR file can hold any form of data, you first need to determine if it holds information that can be visualised in some form, and if so, how? Where every datapoint has a value, latitude and longitude associated with it, the chances are that it can be viewed in some manner.

I found that the best place to start was the *EUMETSAT Product Navigator* with EUMETCAST-Europe and BUFR filters applied so that only the relevant products were listed. From there I would select a product of interest and then select EUMETCast-Europe to reveal the typical file name. Further down the page under 'Resources', there should be links to documents that (hopefully) describe the format of the data. They may also show representative visualisations indicating that a particular product is suitable for this form of interpretation.

BUFRdisplay

Having established that visualisation was feasible, the next step was to try using *BUFRdisplay* to visualise the data. As *BUFRdisplay* is a generic viewer, some effort is required from a user to locate the relevant data and optimise the display after loading a file and decoding the data. Note that I am not attempting to provide a user guide for *BUFRdisplay* (see the official guide for this) but to highlight my experiences.

First, the Data Selection Panel towards the bottom of the *BUFRdisplay* window lists all the variables contained within the BUFR file, the majority of which tend to be metadata containing information about satellite status and data quality. The trick is to locate and select the data field that contains the information to be visualised with the help of the documents identified by the *Product Navigator*. However, just because the data field exists does not mean that it contains any valid data and this must be bourne in mind. *BUFRdisplay* will inform you

if a field has no usable data. Sometimes the same data description appears more than once and closer scrutiny of the documentation and value fields at the bottom of the Data Selection panel may be required to determine the precise nature of the data. As I said, BUFR can be complicated.

As a generic viewer, *BUFRDisplay* has a number of drawbacks in my opinion for ease of use.

1 Although the general configuration of the viewer can be stored as presets for various products, the data field within the Data Selection window cannot be stored and must be selected every time.

2 The data cannot be filtered by quality flags to remove extraneous values from display. This is particularly relevant for scatterometer data (more about this later).

3 For vector displays of wind data, the data cannot be thinned to avoid overcrowding where the data density is particularly high. I do appreciate that without an intimate knowledge of the data structure of a given BUFR file, thinning evenly in two dimensions is not really possible.

4 The map is not interactive once generated. I know that an interactive map is something of a luxury and requires a lot of effort to provide but I do like it as a casual viewer.

5 On zoom levels of 2 or above, the colour bar that provides the visual calibration typically disappears from view when examining areas of interest because it remains located in the bottom left of the unzoomed image.

BUFR Viewer

For vector displays of wind products, I much prefer *BUFR Viewer* as the map display is interactive, data can be thinned and scatterometer data is subject to filtering. Interestingly, *BUFR Viewer* borrows the BUFRextract decoding engine that also underpins *BUFRdisplay*. I use *BUFR Viewer* for scatterometer winds from LEO satellites and Atmospheric Motion Vectors from MSG.

As mentioned at the start of this article, *BUFR Viewer* was unable to display Polar Winds from the LEO METOP satellites because of a format change, so I set about trying to rectify the situation.

Decoding BUFR Data

I noted that the internal interface between the BUFRextract engine and the main *BUFR Viewer* application was via an ASCII text columnar table. Although the BUFRextract decoding engine was able to decode the new Polar Winds format without error, the order of columns had changed which was why the *BUFR Viewer* was not able to display the data. I reasoned that if I could reproduce the original text format, *BUFR Viewer* would work correctly. Rather than trying to parse and modify the intermediate text table, I decided to try and derive this directly from the BUFR data as this would give greater flexibility. but how, as *Python* was the only language with which I stood a chance and not a very good one at that!

The EUMETSAT website gave a few suggestions that included *ecCodes*, pybufrkit, wreport, trollbufr and BUFRextract. I quickly eliminated the middle three due to lack of documentation and knowledge on my behalf. BUFRextract looked feasible but it dumped all the variables into a table and would need additional post-processing which I did not want. This left *ecCodes* provided by the European Centre for Medium Weather Forecasts (ECMWF).

The *ecCodes* software is actually a library for encoding/decoding BUFR data with the majority written in the C and C++ languages which was of no use to me. Fortunately, this library is available with *Python* bindings, or links which allow the decoding functions to be called directly from *Python*. To simplify installation, the *ecCodes*/*Python* combination is available as a Conda package [4] for Windows along with good documentation and working examples on the ECMWF website.

If using the *ecCodes*/*Python* software for decoding, individual variables within a BUFR files are identified by so called keys and these must be identified so that they can be referenced in the *Python* Code. In addition, the structure of the BUFR file needs to be determined. *BUFRdisplay* has the ability to generate a text file detailing the structure and contents of the file but unfortunately, this does not relate to the ECMWF key names. However, ECMWF has another software package called 'codes-ui' that allows the structure of a BUFR file to be examined interactively and also provides the names of the keys. Fortunately, it is also available as a Conda package [5] for Windows with details on the ECMWF website. One point to note is that the Windows is not a native platform for ECMWF so a Windows version may only be provided on a 'best effort' basis. My own experience is that the Linux version of codes-ui works perfectly but that the Windows version has a few rough edges. However, it proved to be adequate for my purposes. Figure 1 (overleaf) shows the structure of a scatterometer BUFR files revealed by codes-ui with the key names. Figure 2 provides a world map showing the location of the observations. The original images have been cropped to focus on the core details.

Once I had established all the key names, I was able to prepare a *Python* script which extracted all the wanted variables from the BUFR file using the *Python* API calls provided by ECMWF. Single variables are returned as numeric *Python* variables. Some BUFR data arew stored in a compressed form and this is extracted in the form of one dimensional

ssage: 1 Subset: 1 subsets: **336** (compressed) (total number of messages: **6**, subsets: **2016**)

dex

Data tree | Descriptors | Compressed | Tables | Debug | Locations

Key	Value	Units	Extra
Header			
Data			
centre	99	CODE TABLE	
subCentre	0	CODE TABLE	
softwareIdentification	1103	Numeric	
satelliteIdentifier	5	CODE TABLE	
satelliteInstruments	190	CODE TABLE	
directionOfMotionOfMovingObservingPlatform	196	deg	
year	2023	a	
month	8	mon	
day	27	d	
hour	12	h	
minute	30	min	
second	0 (336 items)	s	
latitude	46.4315 (336 items)	deg	
longitude	-24.0378 (336 items)	deg	
pixelSizeOnHorizontal1	25000	m	
orbitNumber	24926	Numeric	
crossTrackCellNumber	1 (336 items)	Numeric	
heightOfAtmosphere	missing	m	
lossPerUnitLengthOfAtmosphere	missing	dB/m	
beamCollocation	1	CODE TABLE	
beamIdentifier: 1			
beamIdentifier: 2			
beamIdentifier: 3			
beamIdentifier	3	CODE TABLE	
radarIncidenceAngle	63.64 (336 items)	deg	
antennaBeamAzimuth	248.91 (336 items)	deg	
backscatter	-29.1 (336 items)	dB	
radiometricResolutionNoiseValue	4.3 (336 items)	%	
ascatKpEstimateQuality	0	CODE TABLE	
ascatSigma0Usability	0 (336 items)	CODE TABLE	
ascatUseOfSyntheticData	0	Numeric	
ascatSyntheticDataQuantity	0	Numeric	
ascatSatelliteOrbitAndAttitudeQuality	0	Numeric	
ascatSolarArrayReflectionContamination	0	Numeric	
ascatTelemetryPresenceAndQuality	0	Numeric	
ascatExtrapolatedReferenceFunctionPresence	missing	Numeric	
landFraction	0	Numeric	
softwareIdentification	500	Numeric	
databaseIdentification	3	Numeric	

Figure 1 – Partial structure of BUFR scatterometer file as revealed by Codes-UI

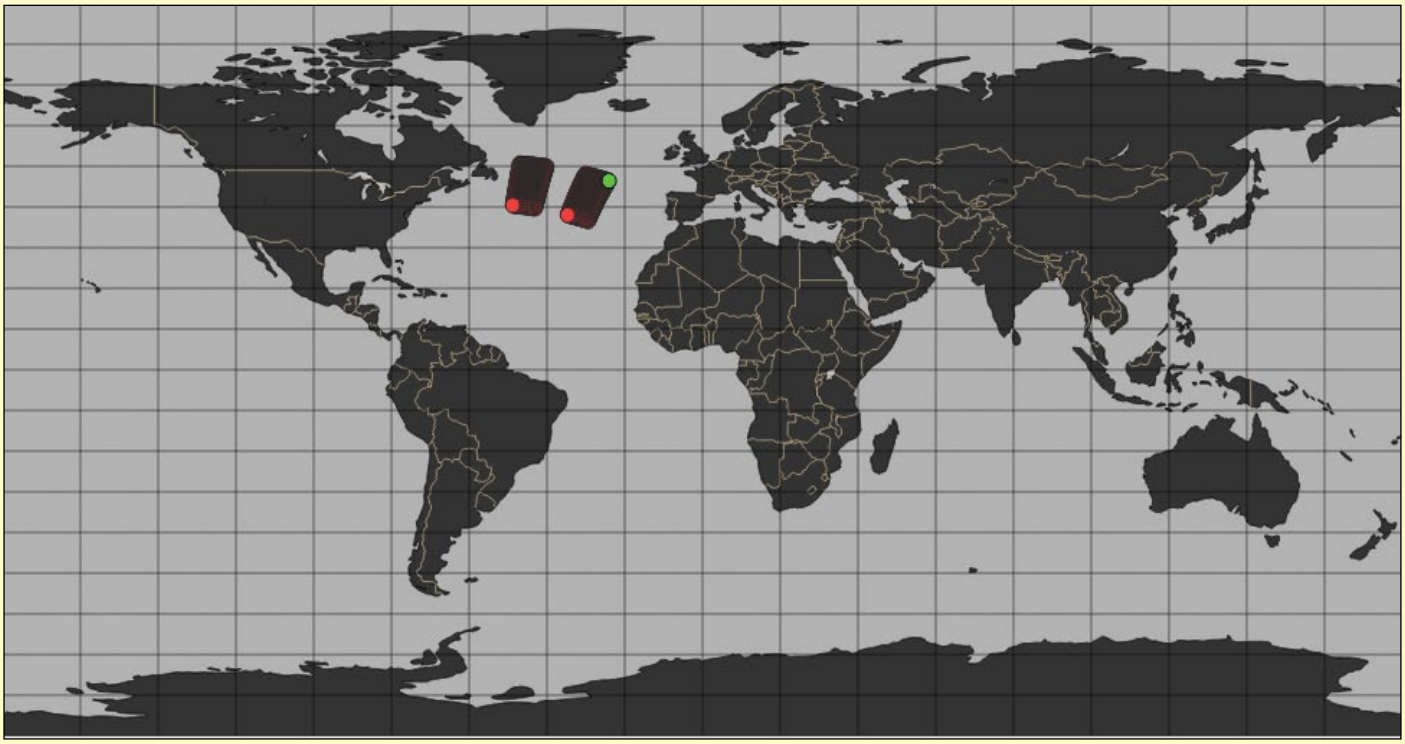

Figure 2 – Observation location map for BUFR scatterometer file produced by Codes-UI

Numpy arrays (Numpy is a *Python* library used for processing datasets in one or more dimensions). Having extracted the data, I wrote it as a text file with columns to match the format and filename expected by *BUFR Viewer*. I then prepared a dummy BUFR file with the same name as the text file (but without the .txt extension) so that *BUFR Viewer* would use this text file instead of trying to decode the BUFR file again.

Viewer Enhancements

With *BUFR Viewer*, only one BUFR file can be selected at a time. However, by using *Python*, I have been able to combine multiple BUFR files from the scatterometer data of LEO satellite to greatly increase the area coverage available on the map display. In addition, I can also add a colour coded windspeed background to the vector display by making use of the background facility provided by *BUFR Viewer*.

For ease of use, I prepared a 'radio button' data selector using the *Python Tkinter* library so that I could select the satellite(s) of interest and the resolution. By default, the data selector uses all files in the reception folder that match the requirement. Figure 3 shows the data selector which allows different combinations of satellites. Figure 4 shows the result of combining multiple METOP B & C files to produce a composite image and Figure 5 shows the same result but with a coloured windspeed overlay.

Viewing Sounder Data

I have access to data from the 22 channel Advanced Technology Microwave Sounder carried on JPSS satellites (currently Suomi NPP, NOAA-20 and NOAA-21) which is transmitted as a BUFR file over EUMETCast-Europe. Whilst this data can be visualised using *BUFRdisplay* using a lot of manual selectionATMS to access the wanted channel, I decided to try an alternative method using the VISAN tool which I described in Geo Newsletter 74. This provides an interactive 3D globe representation.

The data is stored in compressed form within the BUFR file and is extracted as a 1D Numpy array by the ECMWF *Python* code. As a happy coincidence, this format is exactly matches the requirement of the VISAN tool making display of the data a relatively easy task. To simplify the selection of the channel, I constructed a 'radio button' selection window as shown in Figure 6. Following the selection, the *Python* script automatically opens Windows Explorer to show all available files and then invokes the VISAN Tool. An example of an image for channel 16 is shown in Figure 7. Interpretation of the images is another matter....

Meteorological Observations

I use the DWDSAT channel to provide Met Office weather charts as an overlay on visible and infra-

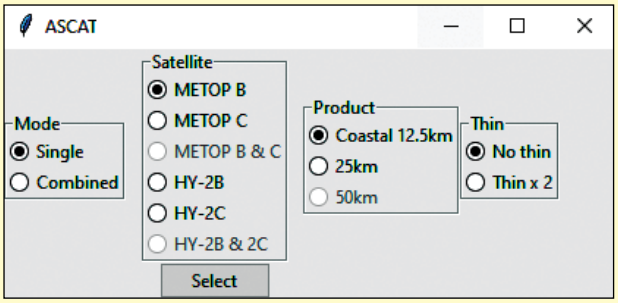

Figure 3 – Selection box for scatterometer observations from METOP and HY-2 LEO satellites

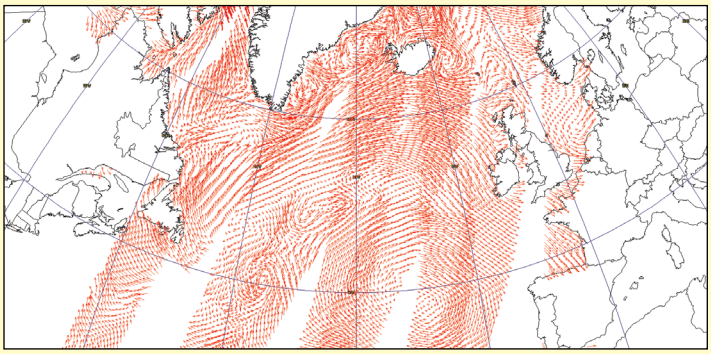

Figure 4 – BUFR Viewer display of multiple scatterometer files from METOP B & C

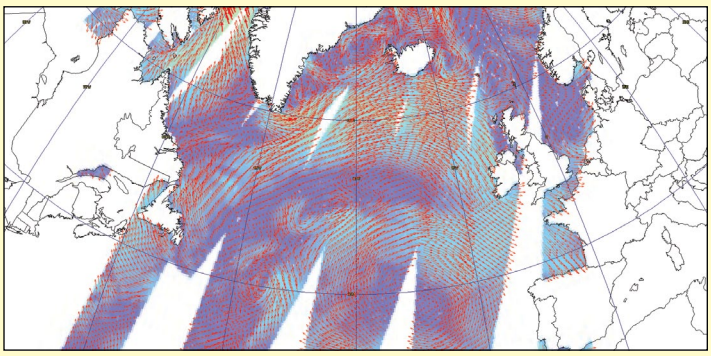

Figure 5 - BUFR Viewer display of multiple scatterometer files from METOP B & C with wind speed overlay

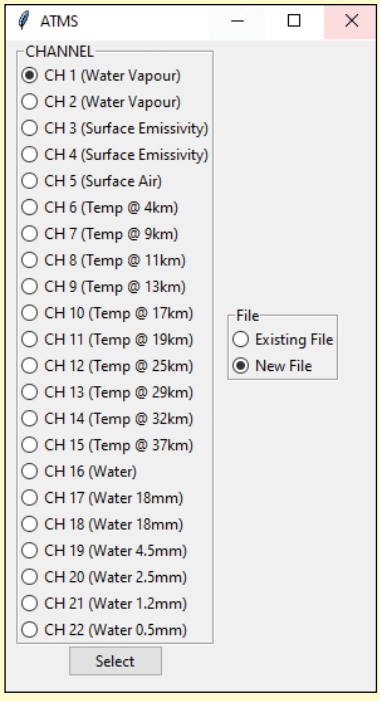

Figure 6 – Selection box for ATMS channel to be displayed. Channel purpose may not be entirely accurate

red images. However, DWDSAT also provides meteorological land surface, sea and upper air observation data from meteorological stations world wide. The Product Navigator for EUMETCast-Europe only identifies DWDSAT as a provider with no detail of the products that it disseminates. For that, it is necessary to interrogate the DWD website directly.

The observational data is provided in two forms which are defined in the World Meterological Organisation (WMO) document No. 306 as follows:-

1 Volume I.1 Part A- Alphanumeric Codes

2 Volume I.2 Part B –Binary Codes (this covers BUFR and GRIB formats)

3 Volume I.3 Part C – Common Features to Binary and Alphanumeric Codes

Some readers may be familiar with the alphanumeric codes which are presented in blocks of five digits and need to be decoded to provide the raw observational data.

DWDSAT transmits the observation data in both formats for some reason, but the majority is in BUFR format and covers land (surface), ship and upper air origins. Unlike satellite observations, the raw data for these transmissions comes from multiple sources so it is provided in the form of BUFR files with uncompressed data as each BUFR message can be different. As noted by Francis Breame, this information is of no use to *BUFRdisplay* is it will only decode the first message. It can be decoded by *BUFRextract* and produced as a text CSV file but this will need additional post processing to extract the relevant data.

Now, decoding the data is all very well but there is little point unless it can be analysed and/or displayed in a meaningful manner, but there are some potential solutions within reach of the amateur.

Alphanumeric Codes

For alphanumeric codes which need no decoding, there appears to be remarkably little software that can handle land, sea and upper air formats. However, one package is able to cope is the venerable Digital Atmosphere [6]. Having said that, I find that its quality control is open to question and features that should work (according to the documentation) do not. For example, I cannot make it display upper air graphs but it does work well for surface and ship observations producing results that will be be familiar to users of this software package. Other software packages are capable of displaying point observations but the alphanumeric codes require decoding first. I have not pursued this path.

Binary Codes

The majority of the metrological observations are transmitted by DWDSAT in BUFR format and I

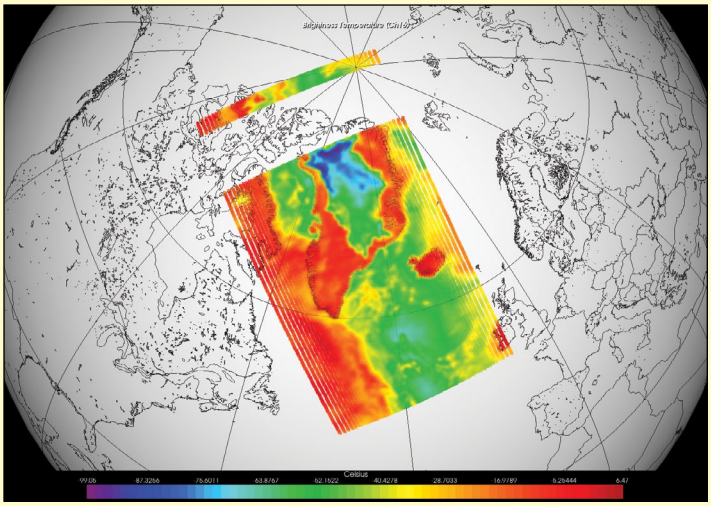

Figure 7 – ATMS Channel 16 data displayed using VISAN

reasoned that it should be possible to produce a text CSV file in a format that *Digital Atmosphere* could understand using *Python* and the *ecCodes* library with a single script. Research revealed that *Digital Atmosphere* recognises observations in a text format provided by the Australian Meteorological bureaux and I set about reproducing this format from the BUFR data. Eventually, I was successful and able to use *Digital Atmosphere* to plot surface and ship observations in the normal matter. Oddly, the most difficult part was dealing with missing data as this could occur at any point and in any message, seemingly at random. Whilst upper air observation data was recognised by *Digital Atmosphere*, it stubbornly refused to plot it but I was determined to find a solution that would.

Upper Air Observations

Typically, upper air observation are plotted in the form of a Tephigram diagram (primary used by the UK Met Office) or a Skew-T diagram which is used elsewhere. These plots show temperature, humidity and wind speed/direction in the atmosphere plotted against atmospheric pressure. I am not describing the format of these plots or their interpretation in this article but I will refer interested readers to Met Office Factsheets [7] and No. 13 in particular.

As I have not found a way to plot the alphanumeric upper air observations, primarily through the lack of decoding software, I have ignored them. For the binary format, as I could use *Python* and the *ecCodes* library to produce a text output in any required format, the hunt was on for suitable software to produce the graphs with the minimum of programming.

Eventually, I identified three possible solutions. The first two were *SHARPPy* and *MetPy*. As the names suggest, these are both *Python* libraries only requiring a steep learning curve and not inconsiderable *Python* knowledge to implement. This did not appear to be a viable solution for me. Eventually, I realised that *McIDAS-V* had a built-in function to generate Skew-T diagrams with the

added bonus of plotting the station locations on a world map—it merely required data in a format that it could recognise.

Even this proved to be a challenge as the only alphanumeric format available was that used by the China Meteorological Administration and I had to ask the providers of the software directly for the relevant details. Once I had this information, I was able to produce the diagrams. Figure 8 shows the interactive map of upper air sounding station locations. Clicking on station 3808 in Cornwall produced the interactive Skew-T diagram shown in Figure 9 and also the interactive Hodograph shown in Figure 10. Once again, interpretation of the images is another matter.

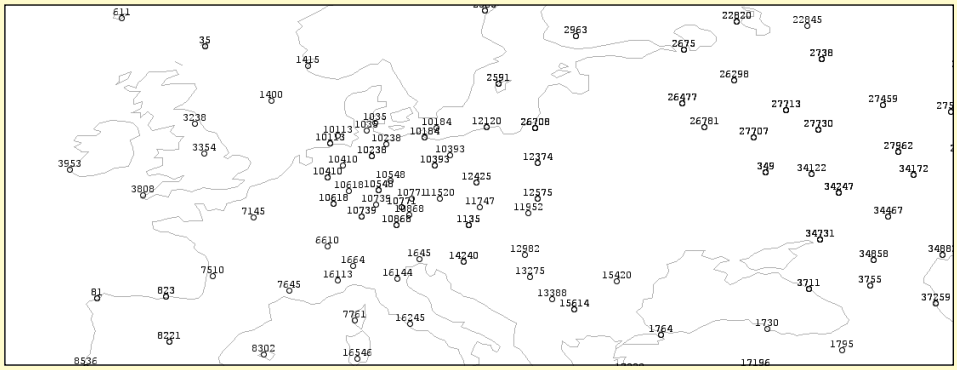

Figure 8 – McIDAS-V interactive map showing upper air observation locations

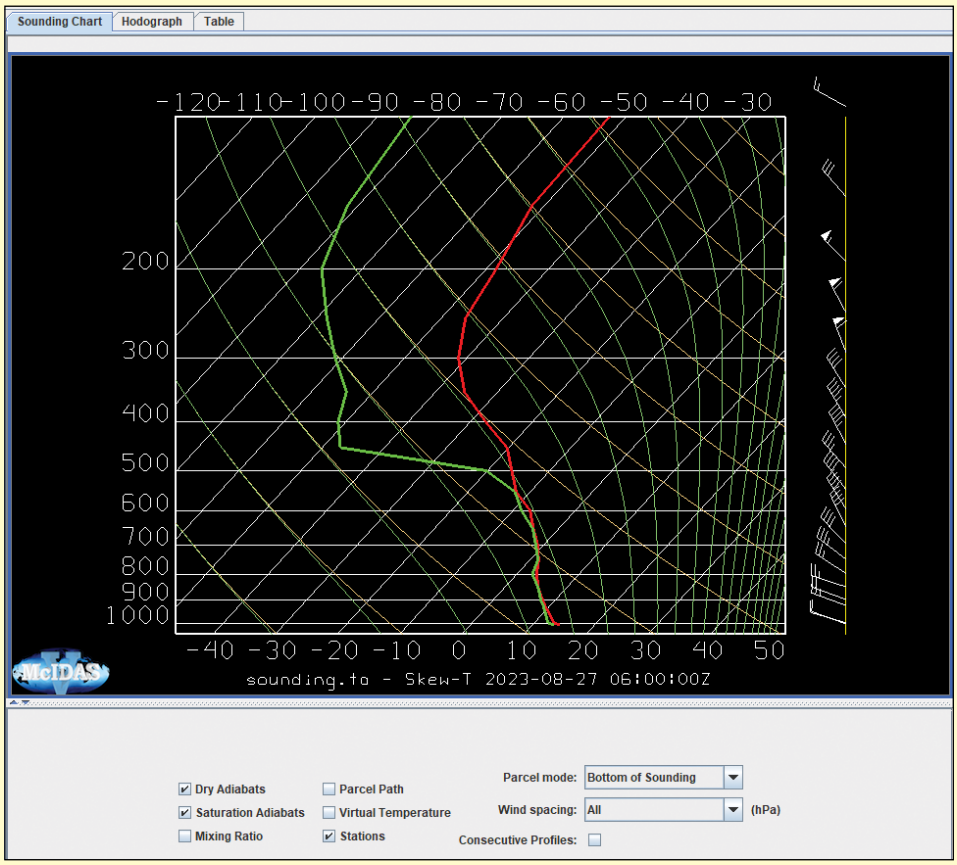

Figure 9 – McIDAS-V Skew-T diagram of upper air measurement from Cornwall

Conclusion

I appreciate that most readers are interested in the direct observations produced by visible and infra-red sensors on the various polar and geostationary satellites. However, I find decoding and visualisation of the multiple formats, typically from derived products, as a challenge in itself and hence my go at BUFR this time round. I have also demonstrated that a small amount of additional software can prevent existing applications from being rendered obsolete because of a change of data format.

References

1 Product Navigator
https://navigator.eumetsat.int/

2 EUMETSAT formats webpage
https://www.eumetsat.int/formats

3 Francis Breame user guides
https://www.elnath.org.uk/

4 ecCodes Conda package
https://anaconda.org/conda-forge/python-eccodes

5 'codes-ui' Conda package
https://anaconda.org/search?q=codes-ui

6 Digital Atmosphere
http://www.weathergraphics.com

7 Met Office Factsheets
https://www.metoffice.gov.uk/research/library-and-archive/publications/factsheets

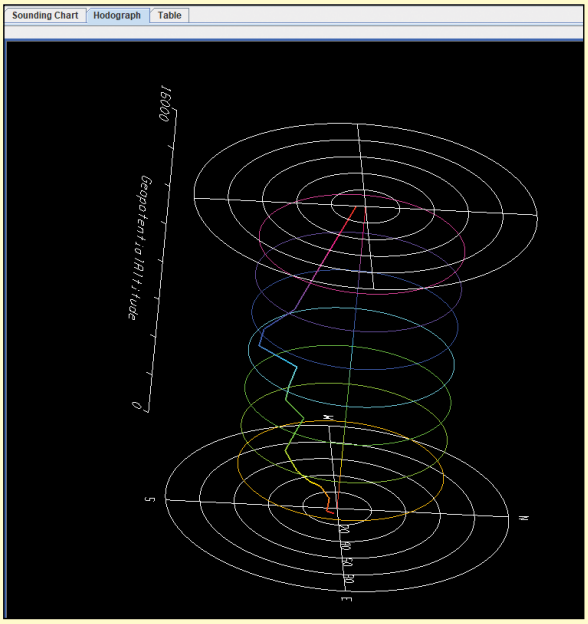

Figure 10 – McIDAS-V Hodograph of upper air measurement from Cornwall

Windpark Fryslân in Lake IJssel, Netherlands

Copernicus Image of the Day

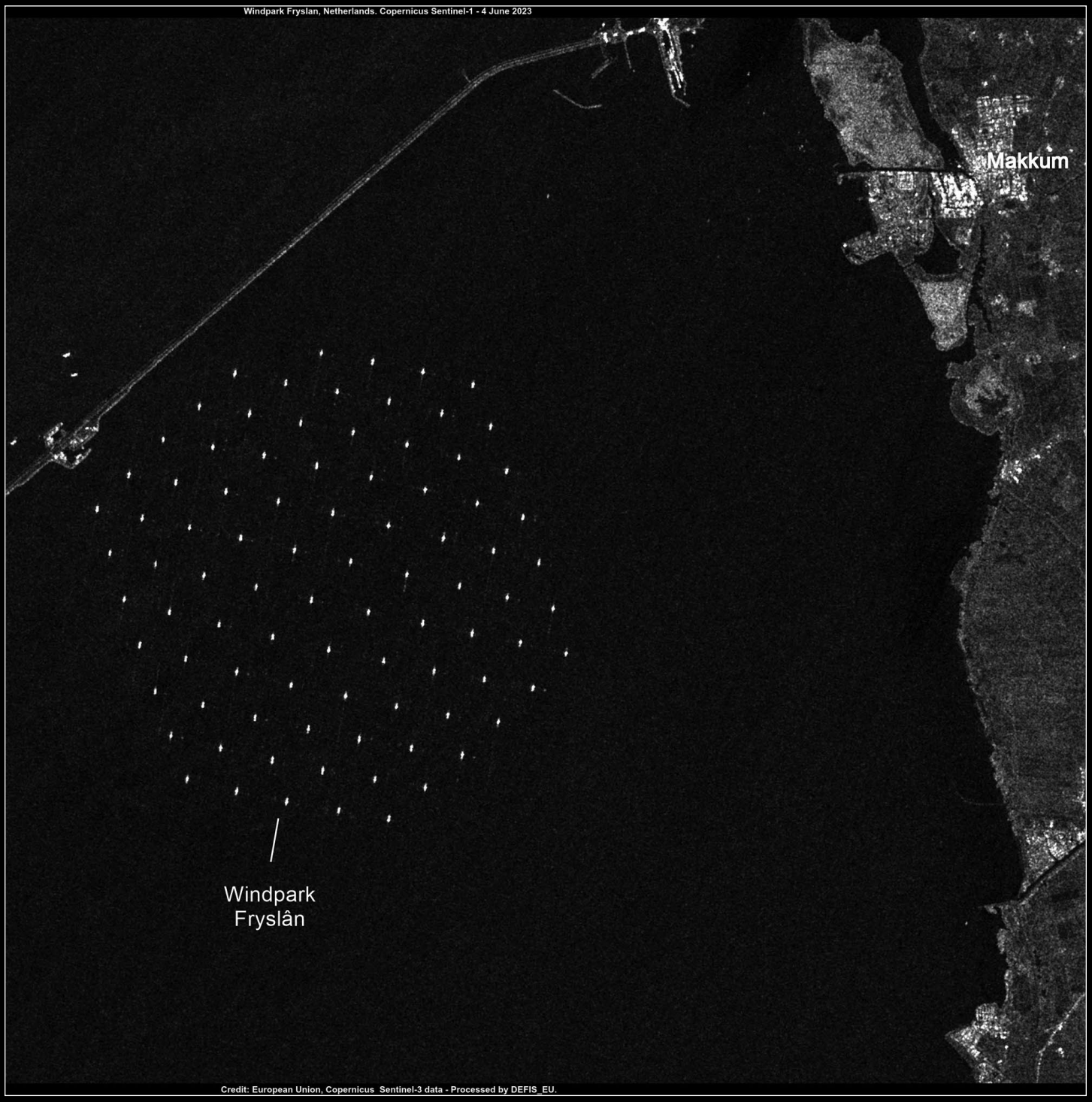

Credit: European Union, Copernicus Sentinel-1 imagery

This image, acquired by the Copernicus Sentinel-1A satellite, shows Windpark Fryslân, the largest freshwater wind farm in the world. The wind turbines were installed in Lake IJssel in the Netherlands, and started running at the end of 2021.

Fryslân has a total power capacity of 382.7 MW. It consists of 89 wind turbines, each with a capacity of 4.3 MW. It is expected to produce approximately 1.5 TWh per year, equivalent to about 1.2% of the electricity consumption in the Netherlands, or the power needs of 500,000 households. This will result in a reduction of 800,000 tonnes of CO2 emissions annually.

The Copernicus Climate Change Service supports the wind energy sector by providing accurate, open data that allows for wind energy stakeholders to make informed decisions in the operation and maintenance of their wind farms in Europe.

July 2023 was the Hottest Month on Record

NASA Earth Observatory

Story by Emily Cassidy

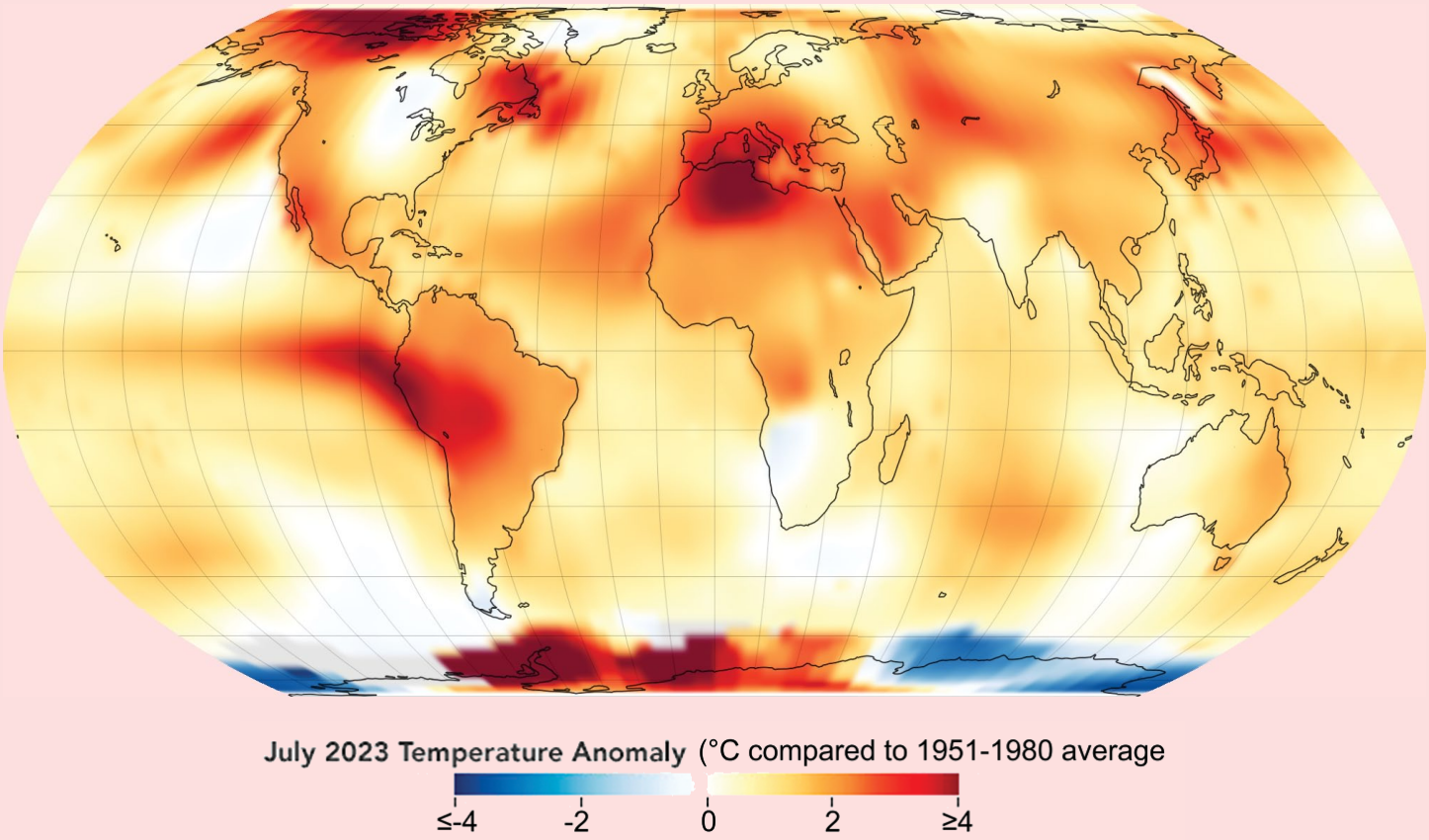

NASA Earth Observatory image by Lauren Dauphin, based on data from the NASA Goddard Institute for Space Studies.

July 2023 was hotter than any other month in the global temperature record, according to an analysis by scientists at NASA's *Goddard Institute for Space Studies* (GISS).

> *'This July was massively warmer than any previous July and any previous month on record, which goes back to 1880,'* said GISS Director Gavin Schmidt. *'This continues the long-term trend in dramatic warming that we have seen over the past four decades.'*

The map above depicts global temperature anomalies for July 2023. It shows how much warmer or cooler the Earth was compared to the baseline average from 1951 to 1980. Note that the deepest reds are at least 4° Celsius above the monthly mean.

Parts of South America, North Africa, North America, and the Antarctic Peninsula were especially hot and experienced temperature anomalies around 4°C. But it was not unusually warm everywhere. Parts of the U.S. Midwest and northern Europe saw closer to average temperatures. Overall, July 2023 was 1.18°C warmer than the average July between 1951 and 1980.

The warmer-than-usual July continues a long-term trend of warming, driven primarily by human-caused greenhouse gas emissions. July 2023 was 0.24°C warmer than any previous July in NASA's record. And according to GISS temperature anomaly data, the top-five hottest Julys since 1880 have all occurred in the past five years.

Extreme heat contributed to devastating wildfires and blistering heat waves in the Northern Hemisphere.

> *'These changes that we're seeing in global temperatures are being reflected in real heat extremes that people are experiencing locally,'* stated Schmidt. *'We can say with some confidence now that the heat waves we are seeing in North Africa, the Middle East, the U.S. Southwest, China, and southern Europe are being directly impacted by the fact that the whole planet is warming.'*

The GISS team assembles its temperature analysis from surface air temperature data from tens of thousands of metrological stations and sea surface temperature data acquired by ship- and buoy-based

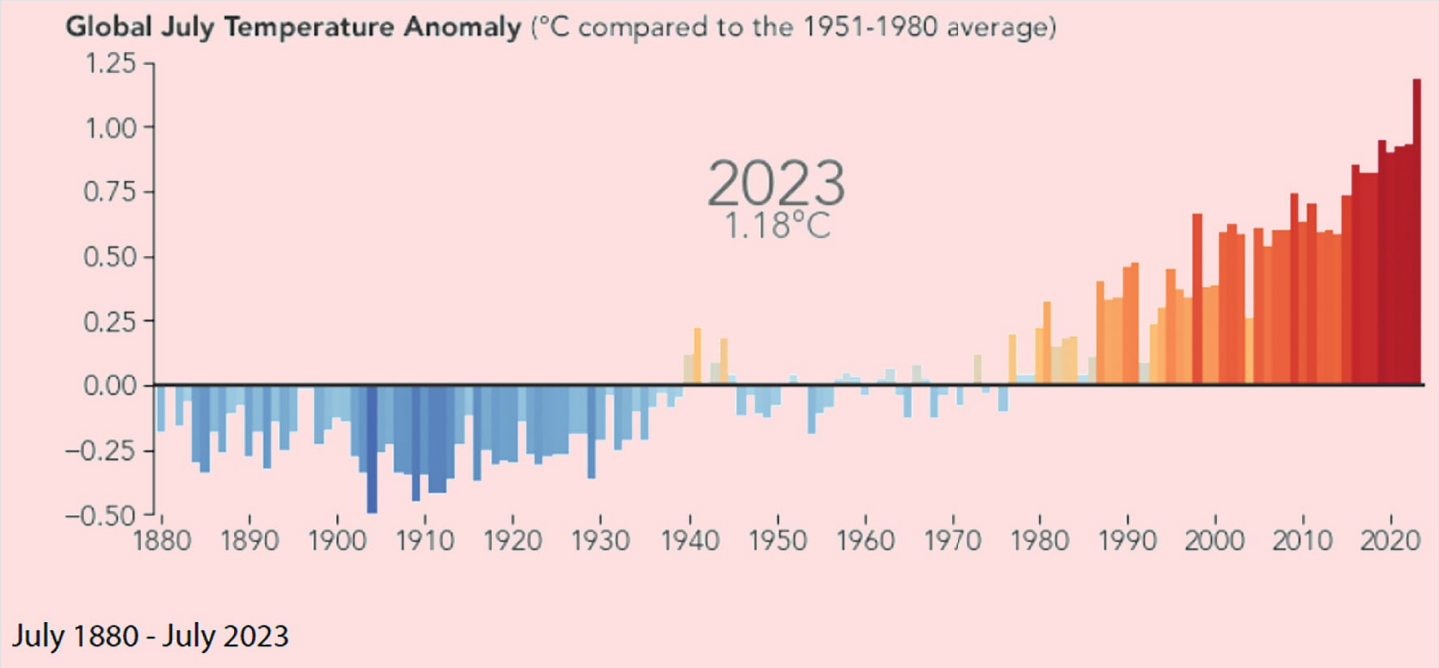

NASA Earth Observatory image by Lauren Dauphin, based on data from the NASA Goddard Institute for Space Studies.

instruments. This raw data is analysed using methods that account for the varied spacing of temperature stations around the globe and for urban heating effects that could skew the calculations.

High sea surface temperatures contributed to July's record warmth. The map shows especially warm ocean temperatures in the eastern tropical Pacific, evidence of the El Niño that began developing in May 2023. Phenomena such as El Niño or La Niña, which warm or cool the tropical Pacific Ocean, can contribute a small amount of year-to-year variability in global temperatures. But these contributions are not typically felt when El Niño starts developing during the Northern Hemisphere's summer.

> *'One of the reasons this record is concerning is that the effects of El Niño on global temperatures normally have a several month lag and are felt in the winter and spring,'* maintained Schmidt. *'Even though we have an El Niño developing now, the record warmth we are seeing is not yet related to that in a significant way. We expect to see the biggest impacts of the developing El Niño in February, March, and April 2024.'*

NASA's full temperature data set and the complete methodology used for the temperature calculation and its uncertainties are available from:

https://data.giss.nasa.gov/gistemp/

Lake Garda continues to be threatened by drought

Copernicus Image of the Day

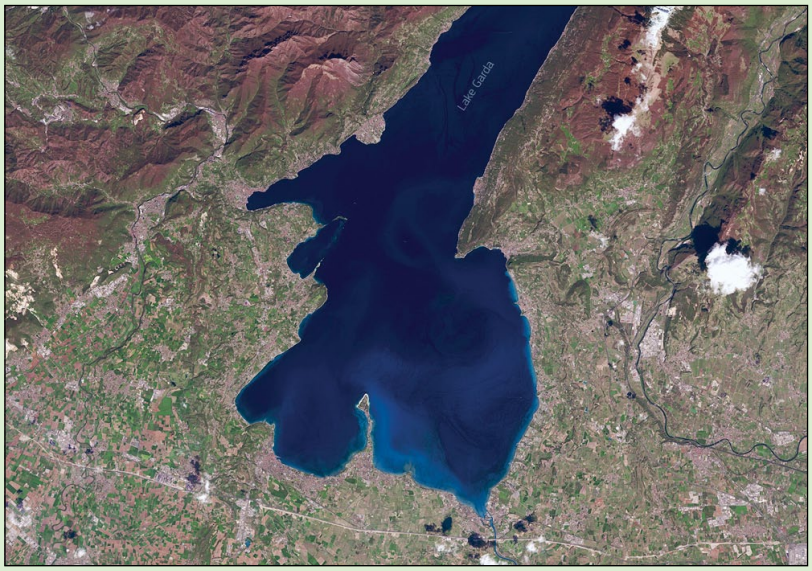

Credit: European Union, Copernicus Sentinel-2 imagery

Italy's longest river, the Po, reached its lowest level ever recorded this April, when water levels in Lake Garda, Italy's largest lake, shown in this Copernicus Sentinel-2 image from April 16, plummeted to their lowest point since 1953. This drop puts water in Lake Garda only 45.8 cm above the hydrometric zero, compared to the 70-year average of 109 cm. As a crucial freshwater reservoir, the current capacity of Lake Garda puts at risk its ability to sustain agriculture, local communities, tourism and navigation.

The Copernicus European Drought Observatory enables accurate monitoring of drought conditions, providing key data for informed decision-making and effective resource management.

Iceland's Fagradalsfjall Volcano Erupts

Copernicus Image of the Day

https://www.copernicus.eu/en/media/image-day

This Copernicus Sentinel-2 image from July 11, 2023 shows the lava flows and the plume emitted by the Fagradalsfjall volcano in Iceland. The eruption began on the same day that this image was acquired, following an intense seismic swarm in the region.

The eruption site is an uninhabited valley near the Litli-Hrútur mountain, approximately 30 kilometres southwest of the capital, Reykjavik. Icelandic authorities have warned tourists and citizens, urging them to stay away from the erupting volcano due to the toxic gas emissions.

Copernicus satellites facilitate the monitoring of volcanic activity worldwide, which is essential for taking action to mitigate the risks and hazards stemming from eruptions.

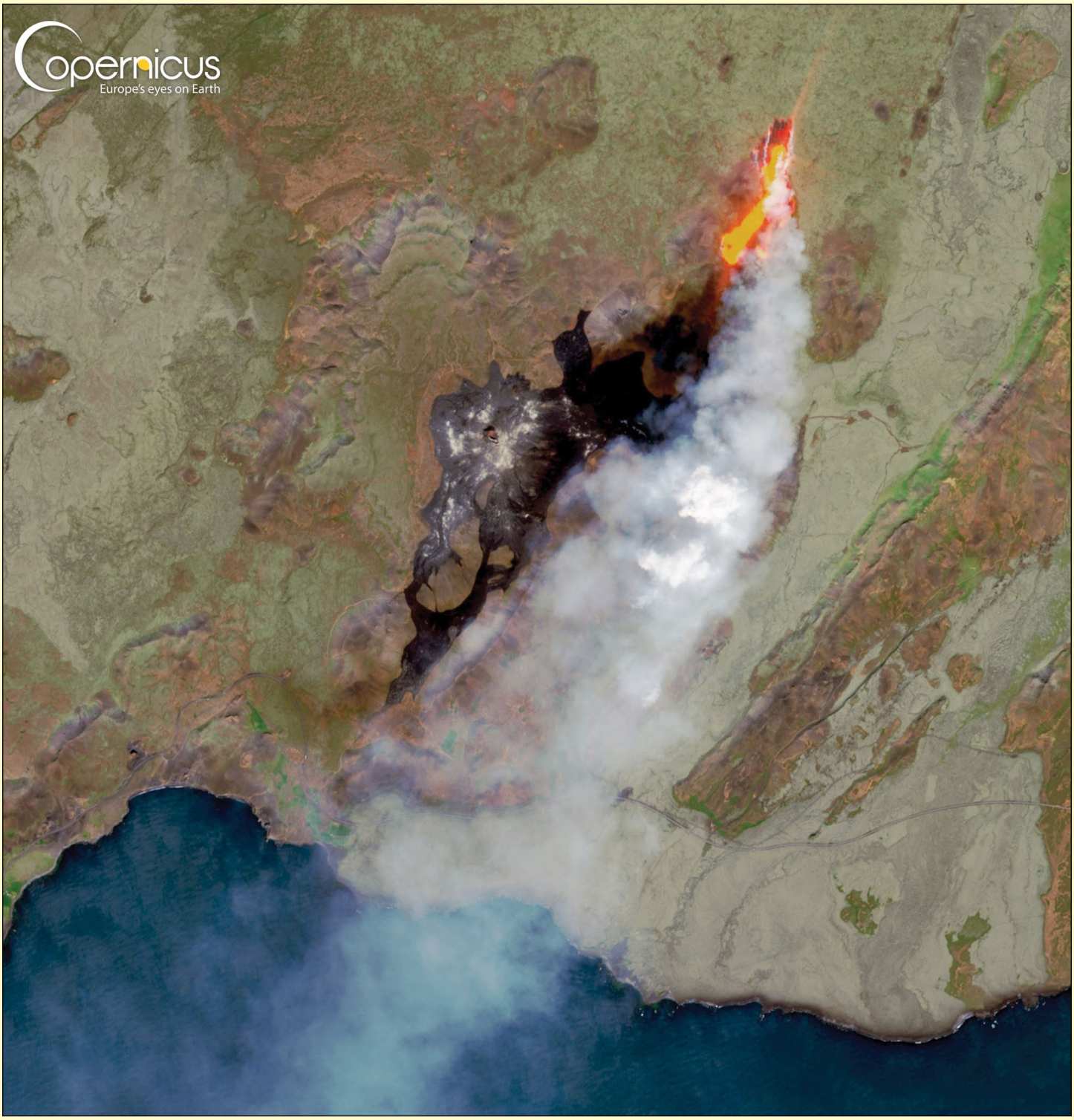

Credit: European Union, Copernicus Sentinel-2 imagery

Meteor M 2-3 Image acquired on August 22, 2023

Ref: article on page 4

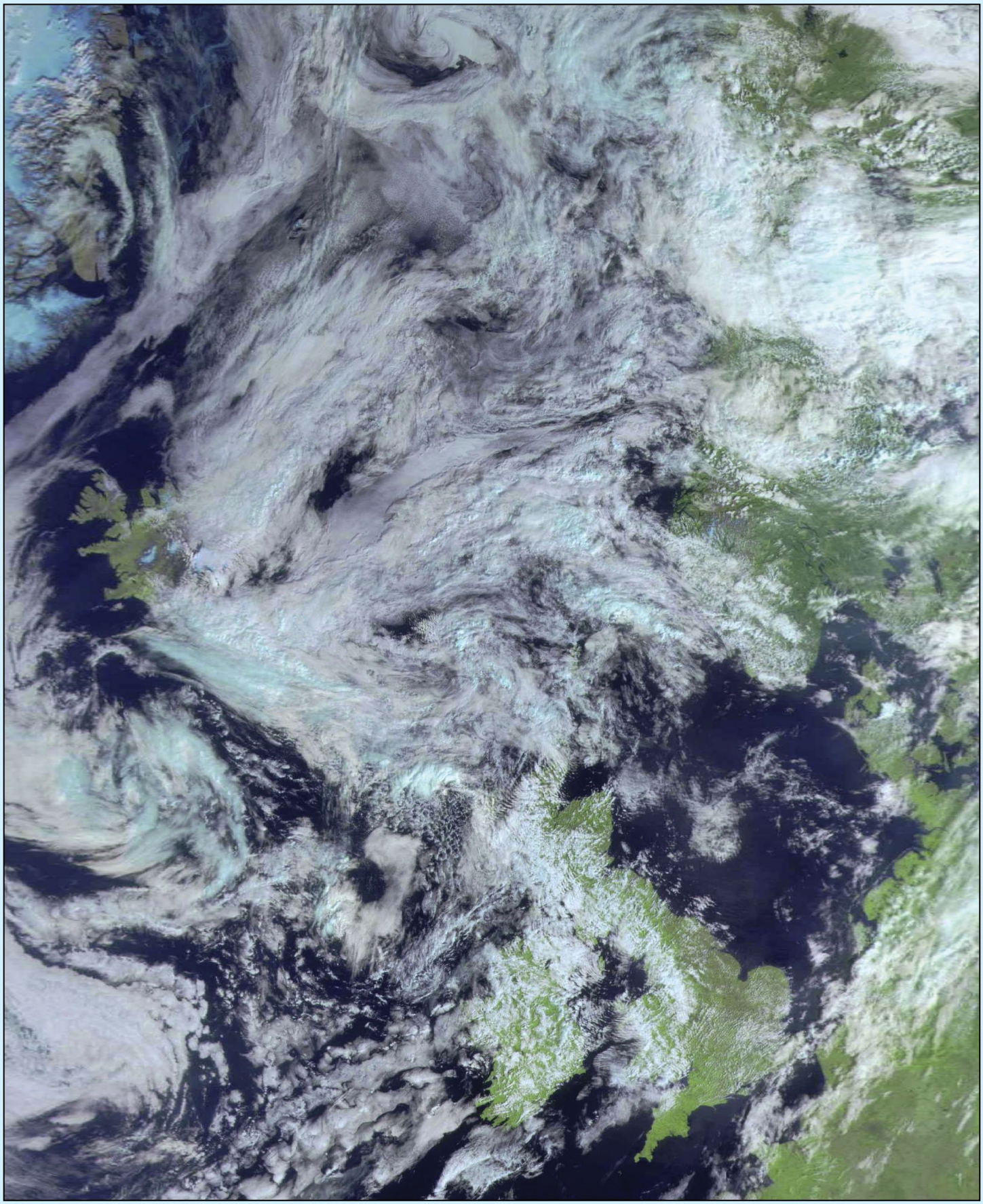

This is a slightly cropped image received in Aberdeen, Scotland at 10.53 UT, from Meteor M 2-3, and at the time, the best so far. But problems still abound, and the following image, received at 12.34 UT, was totally wrecked by three wide black bands!

Wildfires Rage in Greece

NASA Earth Observatory

Text by Kathryn Hansen

NASA Earth Observatory image by Wanmei Liang, using VIIRS data from NASA EOSDIS LANCE, GIBS/Worldview, and the Suomi National Polar-orbiting Partnership.

A month after fires tore across parts of Greece in July 2023, dozens more fires ignited within 24 hours across the country in late August.

A fire in the country's northeast, near Alexandroupolis, produced a plume of smoke that stretched hundreds of miles southwest toward Italy. The plume is visible in this image, acquired in the afternoon on August 22, 2023, by the Visible Infrared Imaging Radiometer Suite (VIIRS) on the NOAA-NASA Suomi NPP satellite.

Smaller plumes are visible from other fires burning elsewhere across the nation. According to news reports, fires near Athens burned homes and cars, and sent smoke wafting over the capital city.

Forecasts called for extreme fire weather—hot, dry, and windy—to continue on August 23. By that day, smoke was detected over Italy and across the Mediterranean Sea in northern Africa.

Fires are not unusual in Greece, but heat-stoked fire weather is projected to become more common as the planet warms. According to data from the European Forest Fire Information System (EFFIS), the area burned in Greece so far in 2023 has surpassed that of the destructive 2021 fire season.

Currently Active Satellites and Freqencies

Polar APT Satellites				
Satellite	**Frequency**	**Status**	**Format**	**Image Quality**
NOAA 15	137.6200 MHz	On	APT	Intermittent sync problem
NOAA 18	137.9125 MHz	On	APT	Good
NOAA 19	137.1000 MHz	On	APT	Good
Meteor M N2	137.1000 MHz	On	LRPT	Failed
Meteor M N2-3	137.9000 MHz	Off	LRPT	Variable [1]

Polar HRPT/AHRPT Satellites				
Satellite	**Frequency**	**Mode**	**Format**	**Image Quality**
NOAA 15	1702.5 MHz	Omni	HRPT	sync problem
NOAA 18	1707.0 MHz	RHCP	HRPT	Good
NOAA 19	1698.0 MHz	RHCP	HRPT	Good
Feng Yun 3C	1701.4 MHz	RHCP	AHRPT	Inactive [2]
Feng Yun 3D	7820.0 MHz	RHCP	AHRPT	Active {2}
Feng Yun 3E	7860.0 Mz	RHCP	AHRPT	Commissioning
Metop B	1701.3 MHz	RHCP	AHRPT	Good
Metop C	1701.3 MHz	RHCP	AHRPT	Good
Meteor M N2-2	1700.0 MHz	RHCP	AHRPT	Active [8]
Meteor M N2-3	1700.0 MHz	RHCP	AHRPT	Active

Geostationary Satellites				
Satellite	**Transmission Mode(s)**		**Position**	**Status**
Meteosat 9	HRIT (digital)		45.5°E	IODC - On
Meteosat 10	HRIT (digital)	LRIT (digital)	9.5 E	Off [4]
Meteosat 11	HRIT (digital)	LRIT (digital)	0°W	On [3]
GOES-13	GVAR 1685.7 MHz	LRIT 1691.0 MHz	61.6°W	[5]
GOES-14	GVAR 1685.7 MHz	LRIT 1691.0 MHz	105°W	Standby
GOES-15 (W)	GVAR 1685.7 MHz	LRIT 1691.0 MHz	128°W	On [6]
GOES-16 (E)	GRB 1686.6 MHz	HRIT 1694.1 MHz	75.2°W	On [7]
GOES-17	GRB 1686.6 MHz	HRIT 1694.1 MHz	137.3°W	On [7]
GOES 18	GRB 1686.6 MHz	HRIT 1694.1 MHz	137.0°W	On [7]
Himawari-8	No direct download	Data is only available via the HimawariCast service	140.7°E	Onw
Himawari-9	No direct download		1450.7°E	On
Feng Yun 2E	SVISSR (digital)	LRIT (digital)	86.5°E	On
Feng Yun 2F	SVISSR (digital)	LRIT (digital)	112.5°E	Standby
Feng Yun 2G	SVISSR (digital)	LRIT (digital)	99.5°E	On
Feng Yun 2H	SVISSR (digital)	LRIT (digital)	79.0°E	On
Feng Yun 4A	HRIT (digital)	LRIT (digital)	99.5°E	On
Feng Yun 4B	HRIT (digital)	LRIT (digital)	Just	Launched

Notes

1 Currently under commissioning, M2-3 regularly swaps both frequency between 137.1 MHz and 137.9 MHz. There are also regular switches in Symbol Rate between 72,000 and 80,000.
2 These satellites employ a non-standard AHRPT format and cannot be received with conventional receiving equipment.
3 Meteosat prime Full Earth Scan (FES) satellite
4 Meteosat prime Rapid Scanning Service (RSS) satellite.
5 Repurposed by US Space Force
6 GOES 15 also transmits EMWIN on 1692.700 MHz GOES 16 also transmits EMWIN on 1694.100 MHz GOES 17 also transmits EMWIN
7 GOES Rebroadcast (GRB) provides the primary relay of full resolution, calibrated, near-real-time direct broadcast space relay of Level lb data from each instrument and Level 2 data from the Geostationary Lightning Mapper (GLM). GRB replaces the GOES VARiable (GVAR) service.
8 Following a collision with a micrometeorite, the power system aboard Meteor M2-2 has been compromised. AHRPT is still being transmitted when the solar panels are sunlit, but there is insufficient battery power to enable the LRPT stream.
9 Japanese satellits MTSAT-1R (Himawari-6) and MTSAT-2 (Himawari-7) are no longer active and are probably retired. Current Japanese operational geostationary satellites are Himawari-8 and Himawari-9).